Research Paper
Computational Methods for Differential Equations
http://cmde.tabrizu.ac.ir
Vol. *, No. *, *, pp. 1-24
DOI:10.22034/cmde.2026.69212.3401

Mathematical analysis of immune response dynamics in Parkinson's disease with Immunotherapeutic intervention

Sunita Chand and Santoshi Panigrahi*
Department of Mathematics, Siksha 'O' Anusandhan (Deemed to be University), Khandagiri Square, Bhubaneswar- 751030, Odisha, India.

Abstract

We develop a fractional-order, time-delay mathematical model of Parkinson's disease that couples neuronal compartments, extracellular α-synuclein, microglial activation and adaptive immune responses. The fractional derivative models long-memory processes (e.g., slow protein aggregation and persistent inflammation) while the discrete delay represents biologically observed lags in immune activation. Parameters were estimated by digitizing published time-series, and the fitted model reproduces the qualitative dynamics reported in the literature. We compute the basic reproduction number $\Re_0$ using the next-generation matrix and perform linear stability and Hopf bifurcation analyses; the first Lyapunov coefficient is negative, indicating a supercritical Hopf bifurcation and the emergence of stable oscillations for sufficiently large delays. Numerical experiments show that increasing the α-synuclein clearance efficacy (ϵ_1) reduces $\Re_0$ and stabilizes the system, whereas microglial and $\mathcal{T}$-cell suppression (ϵ_2, ϵ_3) mainly attenuate oscillation amplitude. Our results support immunotherapeutic strategies that prioritize clearance of pathological α-synuclein to limit disease progression.

Keywords. Parkinson's disease, Fractional-order delay model, Hopf bifurcation, Reproduction number, Immunotherapy.
2010 Mathematics Subject Classification. 34K18, 34K20, 34A08, 92C50, 37G15.

1. Introduction

About seven million people worldwide suffer with Parkinson's disease (PD), which is the second most prevalent progressive neurodegenerative disease (ND) after Alzheimer's disease (AD). It is anticipated that as life expectancy rises, so will the incidence of PD [10]. Movement rigidity and tremors are hallmarks of Parkinson's disease. A part of the brain known as the substantia nigra pars compacta (SNc) exhibits neuronal degeneration. The death of dopaminergic neurons in this area causes the striatum's dopamine (DA) levels to drop, which causes Parkinson's disease's motor symptoms. The goal of current therapy approaches is to raise DA levels by blocking DA-degrading enzymes (e.g., monoamine oxidase blockers) or by directly administering a DA precursor (e.g., L-dopa). In order to functionally compensate for DA depletion, DA receptor agonists are also utilized. Even though these therapies help reduce motor symptoms, they do not modify the underlying disease progression, and therefore PD remains incurable. Age, genetic predisposition, and exposure to environmental pollutants all contribute to Parkinson's disease (PD), a complicated multifactorial illness [6, 16]. About 1% of those over 60 have Parkinson's disease (PD), according to [14]. It results in various cognitive deficiencies and hinders the movement of the upper and lower limbs. One of the most incapacitating symptoms of Parkinson's disease is freezing of gait (FoG). Usually, FoG is seen when the illness is more advanced [11]. It is characterized by an abrupt, involuntary halt to the forward motion of gait. Although PD and indirectly FoG have no known treatment, there are numerous non-invasive ways to manage the condition. In order to control FoG, these choices concentrated on offering aural and sensory cues as well as enhanced feedback [13, 17]. The impact of sensory feedback on normal gait has been extensively studied using mathematical modeling [23, 24].

By removing all toxins from the brain, the immune system safeguards the central nervous system. Damaged neurons are the outcome of inflammations caused by the clearing process. PD may result from neurodegeneration brought

Received: 18 September 2025; Accepted: 13 May 2026.
∗ Corresponding author. Email: santoshipanigrahi@soa.ac.in .

on by the immune system's hyperactive reaction. The effect of the extracellular $\alpha-$synuclein on the development of Parkinson's disease was examined in [4]. The relationship between neurons, extracellular $\alpha-$synuclein, and innate immune response was depicted in the model. The relationship between neurons, extracellular $\alpha-$synuclein, and innate immune response was depicted in the model. As therapeutic measures, a decrease in extracellular $\alpha-$synuclein and a decrease in inflammation brought on by activated microglia in the central nervous system were investigated. We discovered that the latter had no discernible impact in postponing neuronal degeneration. Parkinson's disease is delayed and neurons are preserved by therapies that lower extracellular $\alpha-$synuclein, either by itself or in conjunction with other therapies. The standard procedures for parameter estimation in fractional differential models are discussed in [5, 7, 9, 15, 25]. For fractional epidemic and immune system models, parameter estimations have been described in [3, 27]. Diekmann et al.[8] used the next generation matrix approach to address reproduction number. To asses the robustness of estimated parameters, sensitivity analysis was conducted. On [22, 26], the author's studied the sensitivity analysis of fractional order SVEIR(susceptible–vaccinated–exposed–infected–recovered) Lumpy skin disease and Hepatitis-B disease model respectively. The authors of [2] look into how active and passive immunotherapies can slow the course of Parkinson's disease.

Fractional differential equations have become a rapidly growing area of study due to their numerous applications in a variety of fields[1, 18–21]. In this study, we looked into how active and passive immunotherapies might slow the progression of fractional order Parkinson's disease. Both the innate and adaptive immune responses are included in the model. We use fractional order delay differential equations to simulate the interactions between neurons, activated microglia, extracellular $\alpha-$synuclein, and activated $\mathcal{T}$ cells. Stability analysis is used to investigate how small perturbations influence the behaviour of a dynamical system, while Hopf bifurcation analysis [12] helps identify parameter regimes where delay-induced oscillations emerge. In addition, the basic reproduction number $\Re_0$ is computed using the next-generation matrix method to characterize conditions for disease persistence. A sensitivity analysis based on the normalized forward sensitivity index is then performed to determine the parameters that most strongly influence $\Re_0$. To ensure biological relevance, the model parameters are estimated by fitting the system to digitized experimental data using nonlinear least-squares optimization. These combined analytical and numerical approaches provide a structured framework for understanding the neuroimmune dynamics underlying Parkinson's disease. By combining theoretical results, numerical simulations, and graphical representations of the model, this work offers valuable insight that serves as motivation for our current research. To our knowledge, no such research has been done on the nonlinear fractional order time delay PD model that does stability analysis, Hopf bifurcation analysis, finds the basic reproduction number, performs sensitivity analysis and parameter estimation.

Recent studies in neurodegeneration have demonstrated that neuronal and immunological processes exhibit strong history dependence and non-local temporal interactions. Such long-memory effects arise from phenomena including slow protein aggregation, cumulative oxidative stress, and persistent microglial activation, none of which can be captured adequately by classical integer-order derivatives. Fractional-order models naturally incorporate memory kernels that describe how past states influence present dynamics, making them particularly suitable for biological systems with hereditary properties. In the context of Parkinson's disease (PD), fractional dynamics have been shown to better represent the anomalous diffusion of misfolded α-synuclein, the slow propagation of inflammatory signals, and the gradual degeneration of dopaminergic neurons. In addition, the introduction of a discrete time delay τ is motivated by several biological mechanisms that do not act instantaneously. These include the processing time required for α-synuclein uptake and degradation by microglia, the lag associated with antigen presentation and $\mathcal{T}$-cell activation, and the delayed intracellular transmission of pathogenic α-synuclein species. Incorporating a biologically meaningful delay term allows the model to reproduce such temporal gaps in immune signalling and neuronal response. Together, the fractional-order operator and the discrete delay provide a more realistic representation of the neuroimmune interactions underlying PD progression.

This is how the remainder of the paper is structured. In section 2, the nonlinear fractional order delay Parkinson's disease model is examined, and the existence of a non-negative solution is verified in section 3. In section 4, we calculated equilibrium points such as the disease-free equilibrium and the endemic equilibrium and performed stability and Hopf bifurcation analysis of the model. The basic reproduction number is calculated for the model using the next generation matrix, and sensitivity analysis of the parameters is done in section 5. In section 6, parameter estimation

has been done for the considered model. Section 7 presents numerical simulations that effectively validate our findings. A few closing remarks and general considerations are provided in section 8.

2. Mathematical Model

In [2], a nonlinear time delay mathematical model of PD is covered, which is

$$\mathcal{N}'(t) = \sigma - \beta\mathcal{N}(t)\alpha\mathcal{S}(t) - a_1\mathcal{N}(t) - a_2\mathcal{N}(t) - \mu_1\mathcal{N}(t), \tag{2.1}$$

$$\mathcal{I}'(t) = \beta\mathcal{N}(t)\alpha\mathcal{S}(t) - d_1\mathcal{I}(t) - a_1\mathcal{I}(t) - a_2\mathcal{I}(t), \tag{2.2}$$

$$\alpha\mathcal{S}'(t) = ed_1\mathcal{I}(t) - a_1\alpha\mathcal{S}(t) - a_2\alpha\mathcal{S}(t) - \epsilon_1 ed_1 I(t-\tau)e^{-(a_1+a_2)\tau}, \tag{2.3}$$

$$\mathcal{M}'(t) = a_1\mathcal{I}(t) + a_1\alpha\mathcal{S}(t) - \epsilon_2 a_1(I(t-\tau) + \alpha S(t-\tau))e^{-\mu_2\tau} - \mu_2\mathcal{M}(t), \tag{2.4}$$

$$\mathcal{T}'(t) = a_1\mathcal{I}(t) + (a_1+a_2)\alpha\mathcal{S}(t) - \epsilon_3(a_1\mathcal{I}(t-\tau) + (a_1+a_2)\alpha\mathcal{S}(t-\tau))e^{-\mu_3\tau} - \mu_3\mathcal{T}(t), \tag{2.5}$$

where the variables are defined as:
$\mathcal{N}(t)$: Density of healthy neurons in the brain, $\mathcal{I}(t)$: Density of infected neurons in the brain, $\alpha\mathcal{S}(t)$: Density of extracellular $\alpha-$synuclein in the brain, $\mathcal{M}(t)$: Density of activated microglia, $\mathcal{T}(t)$: Density of activated $\mathcal{T}$ cells.

The parameters are defined as:
σ: Density of new neurons generated per day due to neurogenesis, β: Rate at which neurons become infected, μ_1: Apoptosis rate of healthy neurons, μ_2: Annihilation rate of activated microglia, μ_3: Annihilation rate of activated $\mathcal{T}$ cells, d_1: Death rate of infected neurons due to $\alpha-$synuclein aggregations, a_1: Activation rate of microglia due to extracellular $\alpha-$synuclein and infected neurons, a_2: Activation rate of $\mathcal{T}$ cells due to extracellular $\alpha-$synuclein and infected neurons, e: Percentage of $\alpha-$synuclein that survives following the death of infected neurons, ϵ_1: Percentage of extracellular $\alpha-$synuclein cleared due to immunotherapy, ϵ_2: Percentage of inhibited activated microglia due to immunotherapy, ϵ_3: Percentage of inhibited activated $\mathcal{T}$ cells due to immunotherapy.

The fractional order nonlinear model of PD, including time delays, can be obtained by using the Caputo fractional derivative in the system of Eqs. (2.1)-(2.5), that is,

$$D^q\mathcal{N}(t) = \sigma - \beta\mathcal{N}(t)\alpha\mathcal{S}(t) - a_1\mathcal{N}(t) - a_2\mathcal{N}(t) - \mu_1\mathcal{N}(t), \tag{2.6}$$

$$D^q\mathcal{I}(t) = \beta\mathcal{N}(t)\alpha\mathcal{S}(t) - d_1\mathcal{I}(t) - a_1\mathcal{I}(t) - a_2\mathcal{I}(t), \tag{2.7}$$

$$\alpha D^q\mathcal{S}(t) = ed_1\mathcal{I}(t) - a_1\alpha\mathcal{S}(t) - a_2\alpha\mathcal{S}(t) - \epsilon_1 ed_1 I(t-\tau)e^{-(a_1+a_2)\tau}, \tag{2.8}$$

$$D^q\mathcal{M}(t) = a_1\mathcal{I}(t) + a_1\alpha\mathcal{S}(t) - \epsilon_2 a_1(I(t-\tau) + \alpha S(t-\tau))e^{-\mu_2\tau} - \mu_2\mathcal{M}(t), \tag{2.9}$$

$$D^q\mathcal{T}(t) = a_1\mathcal{I}(t) + (a_1+a_2)\alpha\mathcal{S}(t) - \epsilon_3(a_1 I(t-\tau) + (a_1+a_2)\alpha S(t-\tau))e^{-\mu_3\tau} - \mu_3\mathcal{T}(t), \tag{2.10}$$

with the initial conditions, $\mathcal{N}(0) = \mathcal{N}_0$, $\mathcal{I}(0) = \mathcal{I}_0$, $\alpha\mathcal{S}(0) = \alpha\mathcal{S}_0$, $\mathcal{M}(0) = \mathcal{M}_0$, $\mathcal{T}(0) = \mathcal{T}_0$, where $t \in [-\tau, 0]$, $\tau \geq 0$. The variables and the parameter values as same as described in Eqs. (2.1)-(2.5).

The use of a fractional-order derivative in our model is motivated by the inherently non-Markovian nature of neurodegeneration. Fractional operators allow the rate of change of each state variable to depend on a weighted history of past states, which aligns with experimental evidence indicating that α-synuclein aggregation, microglial priming, and neuronal deterioration accumulate gradually over time. Classical integer-order models assume instantaneous response and therefore may underestimate long-term pathological effects. The discrete delay τ further reflects biologically observed time lags in immune activation pathways, including microglial response time and delayed $\mathcal{T}$-cell recruitment. By incorporating both fractional memory and delayed immune feedback, the model captures the temporally dispersed interactions that drive immune-mediated neuronal damage in Parkinson's disease.

3. Non-negative Solution

To maintain the organic legitimacy of the model, we need to demonstrate that the solutions to the system of differential equations remain positive and bounded for all time estimates. The following lemma outlines the positivity of the solutions in the fractional model.

Lemma 3.1. *The closed set* $\Omega = \{(\mathcal{N}, \mathcal{I}, \alpha\mathcal{S}, \mathcal{M}, \mathcal{T}) \in R^5 : \mathcal{N} + \mathcal{I} + \alpha\mathcal{S} + \mathcal{M} + \mathcal{T} = \frac{\sigma}{\omega}\}$ *is positively invariant with respect to model Eqs.* (2.6)-(2.10).

Proof. By adding Eqs. (2.6)-(2.10), we get

$$\begin{aligned} D^q\mathcal{N}(t) + D^q\mathcal{I}(t) + \alpha D^q\mathcal{S}(t) + D^q\mathcal{M}(t) + D^q\mathcal{T}(t) = \sigma &- (a_1 + a_2 + \mu_1)\mathcal{N}(t) - d_1\mathcal{I}(t) - a_2\mathcal{I}(t) \\ &+ a_1(\alpha\mathcal{S} + \mathcal{I}) + ed_1\mathcal{I} - \mu_2\mathcal{M} - \mu_3\mathcal{T} \\ &- \epsilon_1 ed_1\mathcal{I}(t-\tau)e^{-(a_1+a_2)\tau} \\ &- \epsilon_2 a_1(\mathcal{I}(t-\tau) + \alpha\mathcal{S}(t-\tau))e^{-\mu_2\tau} \\ &- \epsilon_3(a_1(\mathcal{I}(t-\tau) + (a_1+a_2)\alpha\mathcal{S}(t-\tau)))e^{-\mu_3\tau}. \end{aligned}$$

All delay terms in the summed equation appear with negative signs and are multiplied by positive exponential factors $e^{-\mu_i\tau}$ or $e^{-(a_1+a_2)\tau}$, $i = 2, 3$. These terms therefore contribute non positive quantities to $D^qX(t)$ and can be omitted when establishing an upper bound. Since all the parameter values are positive, we get that

$$\begin{aligned} D^q(\mathcal{N} + \mathcal{I} + \alpha\mathcal{S} + \mathcal{M} + \mathcal{T}) &\leq \sigma - \min\{a_1 + a_2 + \mu_1, d_1 + a_2 - a_1 - ed_1, a_1, \mu_2, \mu_3\}(\mathcal{N} + \mathcal{I} + \alpha\mathcal{S} + \mathcal{M} + \mathcal{T}), \\ D^qX &\leq \sigma - \omega X, \end{aligned}$$

where $X = \mathcal{N} + \mathcal{I} + \alpha\mathcal{S} + \mathcal{M} + \mathcal{T}$, $\omega = \min\{a_1 + a_2 + \mu_1, d_1 + a_2 - a_1 - ed_1, a_1, \mu_2, \mu_3\}$.
Solving this equation, we have

$$X(t) \leq \left(-\frac{\sigma}{\omega} + X(0)\right) E_q(-\omega t^q) + \frac{\sigma}{\omega}.$$

Here, $E_q(\cdot)$ denotes the one–parameter Mittag–Leffler function, defined by

$$E_q(z) = \sum_{k=0}^{\infty} \frac{z^k}{\Gamma(kq+1)},$$

which naturally arises in the solutions of linear fractional differential equations. Since, $E_q(-\omega t^q) \geq 0$, when $X(0) \leq \frac{\sigma}{\omega}$. We have

$$\mathcal{N}(t) + \mathcal{I}(t) + \alpha\mathcal{S}(t) + \mathcal{M}(t) + \mathcal{T}(t) = X(t) \leq \frac{\sigma}{\omega}.$$

Hence, $\Omega = \{(\mathcal{N}, \mathcal{I}, \alpha\mathcal{S}, \mathcal{M}, \mathcal{T}) \in R^5_+ : \mathcal{N} + \mathcal{I} + \alpha\mathcal{S} + \mathcal{M} + \mathcal{T} = \frac{\sigma}{\omega}\}$ is positively invariant set with respect to model Eqs. (2.6)-(2.10). □

4. Stability and Bifurcation Analysis

This section provides a comprehensive analysis of stability and bifurcation, incorporating time delay for the model Eqs. (2.6)-(2.10).

4.1. Equilibrium Points.

Let $(\mathcal{N}^*, \mathcal{I}^*, \alpha\mathcal{S}^*, \mathcal{M}^*, \mathcal{T}^*)$ denote the equilibrium point of Eqs. (2.6)-(2.10).

Disease free equilibrium:

Set $\mathcal{I}^* = 0$, $\alpha\mathcal{S}^* = 0$, $\mathcal{M}^* = 0$ and $\mathcal{T}^* = 0$ then Eq. (2.6) gives us $\mathcal{N}^* = \frac{\sigma}{a_1+a_2+\mu_1}$.

So the disease free equilibrium is $\left(\frac{\sigma}{a_1+a_2+\mu_1}, 0, 0, 0, 0\right)$.

Endemic equilibrium:

By equating the right hand side of the Eqs. (2.6)-(2.10) to zero, the equilibrium point is obtained as $E_1 = (\mathcal{N}^*, \mathcal{I}^*, \alpha\mathcal{S}^*, \mathcal{M}^*, \mathcal{T}^*)$, where

$$\mathcal{N}^* = \frac{a_1 + a_2 + d_1}{\beta\left(\frac{ed_1(1-\epsilon_1 e^{-(a_1+a_2)\tau})}{a_1+a_2}\right)},$$

$$\mathcal{I}^* = \frac{\sigma}{d_1 + a_1 + a_2}\left(1 - \frac{(d_1 + a_1 + a_2)(a_1 + a_2 + \mu_1)}{\beta\sigma\left(\frac{ed_1(1-\epsilon_1 e^{-(a_1+a_2)\tau})}{a_1+a_2}\right)}\right),$$

$$\alpha\mathcal{S}^* = \left(\frac{ed_1(1-\epsilon_1 e^{-(a_1+a_2)\tau})}{a_1+a_2}\right)\mathcal{I}^*,$$
$$\mathcal{M}^* = \frac{a_1(1-\epsilon_2 e^{-\mu_2\tau})}{\mu_2}(\mathcal{I}^*+\alpha\mathcal{S}^*),$$
$$\mathcal{T}^* = \frac{1-\epsilon_3 e^{-\mu_3\tau}}{\mu_3}\left(a_1\mathcal{I}^*+(a_1+a_2)\alpha\mathcal{S}^*\right).$$

4.2. **Stability analysis.** Before presenting the detailed derivation, we provide a brief summary of the analytical procedure used to identify the Hopf bifurcation. The analysis begins by linearizing system of Eqs. (2.6)-(2.10) around the endemic equilibrium, which leads to a transcendental characteristic equation due to the presence of the delay τ. A Hopf bifurcation occurs when a conjugate pair of complex eigenvalues crosses the imaginary axis. To determine this point, we substitute $S = i\mathrm{u}$ into the characteristic equation, separate real and imaginary parts, and solve for the critical frequency $\mathrm{u} > 0$ and the corresponding delay value τ_0. The transversality condition is then verified to ensure that the eigenvalues cross the imaginary axis with non-zero speed. The following derivation details these steps.

Let $(\mathcal{N}^*, \mathcal{I}^*, \alpha\mathcal{S}^*, \mathcal{M}^*, \mathcal{T}^*)$ denote the equilibrium point of system of Eqs. (2.6)-(2.10). To analyze the stability of the equilibrium point, we first shift the system so that the equilibrium is translated to the origin. After this change of variables, the system can then be linearized around the origin. Let us define: $\bar{\mathcal{N}} = \mathcal{N} - \mathcal{N}^*$, $\bar{\mathcal{I}} = \mathcal{I} - \mathcal{I}^*$, $\alpha\bar{\mathcal{S}} = \alpha\mathcal{S} - \alpha\mathcal{S}^*$, $\bar{\mathcal{M}} = \mathcal{M} - \mathcal{M}^*$, $\bar{\mathcal{T}} = \mathcal{T} - \mathcal{T}^*$.

$$D^q\bar{\mathcal{N}} = -\beta(\mathcal{N}^*\alpha\bar{\mathcal{S}} + \alpha\mathcal{S}^*\bar{\mathcal{N}}) - a_1\bar{\mathcal{N}} - a_2\bar{\mathcal{N}} - \mu_1\bar{\mathcal{N}}, \tag{4.1}$$
$$D^q\bar{\mathcal{I}} = \beta(\mathcal{N}^*\alpha\bar{\mathcal{S}} + \alpha\mathcal{S}^*\bar{\mathcal{N}}) - d_1\bar{\mathcal{I}} - a_1\bar{\mathcal{I}} - a_2\bar{\mathcal{I}}, \tag{4.2}$$
$$\alpha D^q\bar{\mathcal{S}} = ed_1\bar{\mathcal{I}} - a_1\alpha\bar{\mathcal{S}} - a_2\alpha\bar{\mathcal{S}} - \epsilon_1 ed_1\bar{\mathcal{I}}(t-\tau)e^{-(a_1+a_2)\tau}, \tag{4.3}$$
$$D^q\bar{\mathcal{M}} = a_1\bar{\mathcal{I}} + a_1\alpha\bar{\mathcal{S}} - \epsilon_2 a_1(\bar{\mathcal{I}}(t-\tau) + \alpha\bar{\mathcal{S}}(t-\tau))e^{-\mu_2\tau} - \mu_2\bar{\mathcal{M}}, \tag{4.4}$$
$$D^q\bar{\mathcal{T}} = a_1\bar{\mathcal{I}} + (a_1+a_2)\alpha\bar{\mathcal{S}} - \epsilon_3(a_1\bar{\mathcal{I}}(t-\tau) + (a_1+a_2)\alpha\bar{\mathcal{S}}(t-\tau))e^{-\mu_3\tau} - \mu_3\bar{\mathcal{T}}. \tag{4.5}$$

Taking Laplace transform of Eqs. (4.1)-(4.5) on both sides, we get,

$$\Delta(S)\begin{pmatrix} X_1(S)\\ X_2(S)\\ \alpha X_3(S)\\ X_4(S)\\ X_5(S)\end{pmatrix} = \begin{pmatrix} K_1(S)\\ K_2(S)\\ K_3(S)\\ K_4(S)\\ K_5(S)\end{pmatrix}, \tag{4.6}$$

where, $L\left[\bar{\mathcal{N}}(t)\right] = X_1(S)$, $L\left[\bar{\mathcal{I}}(t)\right] = X_2(S)$,$L\left[\alpha\bar{\mathcal{S}}(t)\right] = \alpha X_3(S)$, $L\left[\bar{\mathcal{M}}(t)\right] = X_4(S)$, $L\left[\bar{\mathcal{T}}(t)\right] = X_5(S)$, $\bar{\mathcal{N}}(0) = \phi_1(0)$,$\bar{\mathcal{I}}(0) = \phi_2(0)$, $\alpha\bar{\mathcal{S}}(0) = \alpha\phi_3(0)$, $\bar{\mathcal{M}}(0) = \phi_4(0)$, $\bar{\mathcal{T}}(0) = \phi_5(0)$,

$$\Delta(S) = \begin{pmatrix} S^q+\beta\alpha\mathcal{S}^*+E+\mu_1 & 0 & \beta\mathcal{N}^* & 0 & 0\\ -\beta\alpha\mathcal{S}^* & S^q+d_1+E & -\beta\mathcal{N}^* & 0 & 0\\ 0 & -ed_1+\epsilon_1 ed_1 e^{-E\tau}e^{-S\tau} & S^q+E & 0 & 0\\ 0 & -a_1+\epsilon_2 a_1 e^{-\mu_2\tau}e^{-S\tau} & -a_1+\epsilon_2 a_2 e^{-\mu_2\tau}e^{-S\tau} & S^q+\mu_2 & 0\\ 0 & -a_1+\epsilon_3 a_1 e^{-\mu_3\tau}e^{-S\tau} & -E+\epsilon_3 E e^{-\mu_3\tau}e^{-S\tau} & 0 & S^q+\mu_3\end{pmatrix},$$

in which $a_1+a_2 = E$, $K_1(S) = S^{q-1}\phi_1(0)$, $K_2(S) = S^{q-1}\phi_2(0)$,
$K_3(S) = \alpha S^{q-1}\phi_3(0) - \epsilon_1 ed_1 e^{-(E)\tau}e^{-S\tau}\int_{-\tau}^{0} e^{-S\tau}\bar{\mathcal{I}}(t)dt$,
$K_4(S) = S^{q-1}\phi_4(0) - \epsilon_2 a_1 e^{-\mu_2\tau}e^{-S\tau}\int_{-\tau}^{0} e^{-S\tau}\bar{\mathcal{I}}(t)dt - \epsilon_2 a_1 e^{-\mu_2\tau}e^{-S\tau}\int_{-\tau}^{0} e^{-S\tau}\alpha\bar{\mathcal{S}}(t)dt$,
$K_5(S) = S^{q-1}\phi_5(0) - \epsilon_3 a_1 e^{-\mu_3\tau}e^{-S\tau}\int_{-\tau}^{0} e^{-S\tau}\bar{\mathcal{I}}(t)dt - \epsilon_3(E)e^{-\mu_3\tau}e^{-S\tau}\int_{-\tau}^{0} e^{-S\tau}\alpha\bar{\mathcal{S}}(t)dt$.

$\Delta(S)$ is considered as characteristic matrix of system of Eqs. (2.6)-(2.10). For notational convenience, we define $E = a_1 + a_2$, representing the combined immune activation rate contributed by microglia and $\mathcal{T}$-cells.

The characteristic polynomial of Eqs. (2.6)-(2.10), is

$$F(S) = Q_1(S) + Q_2(S)e^{-S\tau} + Ce^{-S\tau} = 0, \tag{4.7}$$

where,

$$Q_1(S) = \alpha S^{5q} + D_1 S^{4q} + D_2 S^{3q} + D_3 S^{2q} + D_4 S^q + D_5,$$
$$Q_2(S) = G_1 S^{3q} + G_2 S^{2q} + G_3 S^q,$$
$$C = \epsilon_1 e d_1 e^{-(E)\tau}\mu_2\mu_3(\beta^2\alpha^2\mathcal{S}^*\mathcal{N}^* + \beta\mathcal{N}^*(E+\mu_1)) - \mu_2\mu_3\beta^2\epsilon_1 e d_1 e^{-(E)\tau}.$$

Let $S = iu = u\left(\cos\left(\frac{\pi}{2}\right) + i\sin\left(\frac{\pi}{2}\right)\right)$, where $u > 0$. After substituting S in Eq. (4.7), we get that,

$$A_1 + iB_1 + (A_2 + iB_2)e^{-u\tau} + Ce^{-iu\tau} = 0. \tag{4.8}$$

where A_1, A_2 be the real parts of $Q_1(S)$, $Q_2(S)$, B_1, B_2 are the imaginary parts of $Q_1(S)$, $Q_2(S)$ respectively. A_1, A_2, B_1, B_2 defined as follows:

$$A_1 = u^{5q}\cos\frac{5q\pi}{2} + D_1 u^{4q}\cos\frac{4q\pi}{2} + D_2 u^{3q}\cos\frac{3q\pi}{2} + D_3 u^{2q}\cos\frac{2q\pi}{2} + D_4 u^q\cos\frac{q\pi}{2} + D_5,$$
$$B_1 = u^{5q}\sin\frac{5q\pi}{2} + D_1 u^{4q} sin\frac{4q\pi}{2} + D_2 u^{3q} sin\frac{3q\pi}{2} + D_3 u^{2q} sin\frac{2q\pi}{2} + D_4 u^q sin\frac{q\pi}{2} + D_5,$$
$$A_2 = G_1 u^{3q}\cos\frac{3q\pi}{2} + G_2 u^{2q}\cos\frac{2q\pi}{2} + G_3 u^q\cos\frac{q\pi}{2},$$
$$B_2 = G_1 u^{3q} sin\frac{3q\pi}{2} + G_2 u^{2q} sin\frac{2q\pi}{2} + G_3 u^q sin\frac{q\pi}{2},$$

where

$$D_1 = d_1 + E + \beta q\mathcal{S}^* + E + \mu_1 + \mu_2 + \mu_3,$$
$$D_2 = \mu_2\mu_3(d_1 + E + \beta\alpha\mathcal{S}^* + E + \mu_1) + \mu_2\mu_3 - ed_1\beta\mathcal{N}^*,$$
$$D_3 = (E)(\beta\alpha\mathcal{S}^*(d_1+E) + a_1d_1 + a_1^2 + a_1a_2 + a_2d_1 + a_1a_2 + a_2^2 + \mu_1d_1 + \mu_1a_1 + \mu_1a_2)$$
$$+ (\mu_2\mu_3d_1 + \mu_2\mu_3a_1 + \mu_2\mu_3a_2 + \mu_2\mu_3\beta\alpha\mathcal{S}^* + \mu_2\mu_3a_1 + \mu_2\mu_3a_2 + \mu_1\mu_2\mu_3)$$
$$+ \mu_1d_1 + \mu_1a_1 + \mu_1a_2 - \beta^2\alpha\mathcal{S}^*\mathcal{N}^*ed_1 - \beta\mathcal{N}^*(\mu_2+\mu_3)ed_1 + \beta^2\alpha\mathcal{S}^*\mathcal{N}^*ed_1,$$
$$D_4 = (E)(\mu_2+\mu_3)(\beta\alpha\mathcal{S}^*(d_1+E) + (a_1d_1 + a_1^2 + a_1a_2) + (a_2d_1 + a_1a_2 + a_2^2)$$
$$+ (\mu_1d_1 + \mu_1a_1 + \mu_1a_2)) - (\beta^2\alpha\mathcal{S}^*\mathcal{N}^* + \beta\mathcal{N}^*(E+\mu))(\mu_2+\mu_3)ed_1 + \beta^2\alpha\mathcal{S}^*\mathcal{N}^*ed_1(\mu_2+\mu_3),$$
$$D_5 = (a_1\mu_2\mu_3 + a_2\mu_2\mu_3)(\beta\alpha\mathcal{S}^*(d_1+E) + (a_1d_1 + a_1^2 + a_1a_2) + (a_2d_1 + a_1a_2 + a_2^2)$$
$$+ (\mu_1d_1 + \mu_1a_1 + \mu_1a_2)) - \mu_2\mu_3(\beta^2\alpha\mathcal{S}^*\mathcal{N}^* + \beta\mathcal{N}^*(E+\mu_1))ed_1 + \mu_2\mu_3\beta^2\alpha\mathcal{S}^*\mathcal{N}^*ed_1,$$
$$G_1 = \epsilon_1 e d_1 e^{-(E)\tau}\beta\mathcal{N}^*,$$
$$G_2 = \beta\mathcal{N}^*(E+\mu_1)\epsilon_1 e d_1 e^{-(E)\tau} + \epsilon_1 e d_1\beta\mathcal{N}^*(\mu_2+\mu_3)e^{-(E)\tau} - \beta^2\epsilon_1 e d_1 e^{-(E)\tau},$$
$$G_3 = \beta^2\alpha\mathcal{S}^*\mathcal{N}^* + \beta\mathcal{N}^*(E+\mu_1)(\mu_2+\mu_3)\epsilon_1 e d_1 e^{-(E)\tau} - \beta^2\epsilon_1 e d_1(\mu_2+\mu_3)e^{-(E)\tau}.$$

Now we isolated real and imaginary part of Eq. (4.8) and we get,

$$A_2\cos u\tau + B_2 sinu\tau = -(A_1 + C\cos u\tau), \tag{4.9}$$
$$B_2\cos u\tau - A_2 sinu\tau = -(B_1 - Csinu\tau). \tag{4.10}$$

By squaring both sides of above two equations we get,

$$A_2^2 + B_2^2 - A_1^2 - B_1^2 - C^2 = 2C[A_1\cos u\tau - B_1 sinu\tau]. \tag{4.11}$$

Letting $\cos(u\tau) = h_1(u)$, $\sin(u\tau) = h_2(u)$, with $h_1^2 + h_2^2 = 1$, Eq. (4.11) reduces to the quadratic

$$L_1h_1(u)^2 + L_2h_1(u) + L_3 = 0,$$

where

$$L_1 = 4C^2(A_2^2 + B_2^2), \qquad L_2 = -4CA_1(A_2^2 + B_2^2 - A_1^2 - B_1^2 - C^2),$$
$$L_3 = (A_1^2 + B_1^2 - A_2^2 - B_2^2 - C^2)^2 - 4C^2B_1^2.$$

Thus the critical delays are obtained from

$$\tau_k = \frac{1}{\mathrm{u}}\big(\arccos(h_1(\mathrm{u})) + 2k\pi\big), \qquad k = 0, 1, 2, \ldots, \tag{4.12}$$

and the smallest positive value is taken as the Hopf bifurcation point τ_0.

Theorem 4.1. *When $\tau < \tau_0$, the endemic equilibrium*

$$E_1 = (\mathcal{N}^*, \mathcal{I}^*, \alpha\mathcal{S}^*, \mathcal{M}^*, \mathcal{T}^*)$$

of system of Eqs. (2.6)-(2.10) is locally asymptotically stable.

Proof. To analyze the stability of E_1, we linearize system of Eqs. (2.6)-(2.10) around the endemic equilibrium, which yields the characteristic equation

$$F(S, \tau) = 0.$$

For $\tau = 0$, all characteristic roots satisfy $\Re(S) < 0$, implying that E_1 is locally asymptotically stable in the absence of delay.

Next, assume that $S = i\mathrm{u}$ ($\mathrm{u} > 0$) is a purely imaginary root. Substituting $S = i\mathrm{u}$ into the characteristic equation leads to the real and imaginary parts given in Eqs. (4.9)-(4.11). Solving these equations yields the critical delay τ_0 at which a pair of complex conjugate roots may cross the imaginary axis.

For all delays $0 \le \tau < \tau_0$, no characteristic root crosses into the right half of the complex plane, and therefore all roots satisfy $\Re(S) < 0$. Hence, no oscillatory instability occurs for $\tau < \tau_0$, and the endemic equilibrium E_1 remains locally asymptotically stable.

This completes the proof. □

4.3. **Hopf bifurcation analysis.** To determine the direction and stability of the Hopf bifurcation identified in the previous subsection, we apply the center manifold theorem and normal form theory for delay differential equations. These methods reduce the infinite-dimensional system to a two-dimensional system on the center manifold near the bifurcation point. The sign of the first Lyapunov coefficient determines whether the Hopf bifurcation is supercritical (yielding stable periodic solutions) or subcritical (yielding unstable periodic solutions). The subsequent calculations follow the classical approach of Hassard et al.[12] and provide the explicit expression for the coefficient.

The direction of bifurcation:

$$\frac{dS}{d\tau} = -\frac{F_\tau}{F_S} = \frac{S[Q_2(S)e^{-S\tau} + Ce^{-S\tau}]}{Q_1'(S) + Q_2'(S)e^{-S\tau} - \tau Q_2(S)e^{-S\tau} - \tau Ce^{-S\tau}}. \tag{4.13}$$

Now,

$$\begin{aligned}
S[Q_2(S)e^{-S\tau} + Ce^{-S\tau}] &= (i\mathrm{u})[Q_2(S)e^{-i\mathrm{u}\tau} + Ce^{-i\mathrm{u}\tau}] \\
&= (i\mathrm{u})\left\{G_1\mathrm{u}^{3q}\left[\cos\frac{3q\pi}{2}\cos\mathrm{u}\tau + \sin\frac{3q\pi}{2}\sin\mathrm{u}\tau\right]\right\} \\
&+ (i\mathrm{u})\left\{iG_1\mathrm{u}^{3q}\left[-\cos\frac{3q\pi}{2}\sin\mathrm{u}\tau + \sin\frac{3q\pi}{2}\cos\mathrm{u}\tau\right]\right\} \\
&= (i\mathrm{u})\left\{G_2\mathrm{u}^{2q}\left[\cos\frac{2q\pi}{2}\cos\mathrm{u}\tau + \sin\frac{2q\pi}{2}\sin\mathrm{u}\tau\right]\right\} \\
&+ (i\mathrm{u})\left\{iG_2\mathrm{u}^{2q}\left[-\cos\frac{2q\pi}{2}\sin\mathrm{u}\tau + \sin\frac{2q\pi}{2}\cos\mathrm{u}\tau\right]\right\}
\end{aligned}$$

$$
\begin{aligned}
&+ (iu)\left\{G_3 u^q \left[\cos\frac{q\pi}{2}\cos u\tau + \sin\frac{q\pi}{2}\sin u\tau\right]\right\}\\
&+ (iu)\left\{iG_3 u^q \left[-\cos\frac{q\pi}{2}\sin u\tau + \sin\frac{q\pi}{2}\cos u\tau\right]\right\}\\
&+ (iu)\left\{C\cos u\tau - iC\sin u\tau\right\}\\
&= M_1 + iM_2, \qquad (4.14)
\end{aligned}
$$

where,

$$
\begin{aligned}
M_1 &= G_1 u^{3q+1}\left[\cos\frac{3q\pi}{2}\sin u\tau - \sin\frac{3q\pi}{2}\cos u\tau\right]\\
&+ G_2 u^{2q+1}\left[\cos\frac{2q\pi}{2}\sin u\tau - \sin\frac{2q\pi}{2}\cos u\tau\right]\\
&+ G_3 u^{q+1}\left[\cos\frac{q\pi}{2}\sin u\tau - \sin\frac{q\pi}{2}\cos u\tau\right] + uC\sin u\tau,\\
M_2 &= G_1 u^{3q+1}\left[\sin\frac{3q\pi}{2}\sin u\tau + \cos\frac{3q\pi}{2}\cos u\tau\right]\\
&+ G_2 u^{2q+1}\left[\sin\frac{2q\pi}{2}\sin u\tau + \cos\frac{2q\pi}{2}\cos u\tau\right]\\
&+ G_3 u^{q+1}\left[\sin\frac{q\pi}{2}\sin u\tau + \cos\frac{q\pi}{2}\cos u\tau\right] + uC\cos u\tau.
\end{aligned}
$$

Now, consider the denominator of (4.13),

$$
\begin{aligned}
&Q_1'(S) + Q_2'(S)e^{-S\tau} - \tau Q_2(S)e^{-S\tau} - \tau Ce^{-S\tau}\\
&= 5qu^{5q-1}\left[\cos\frac{(5q-1)\pi}{2} + i\sin\frac{(5q-1)\pi}{2}\right]\\
&+ 4qu^{4q-1}D_1\left[\cos\frac{(4q-1)\pi}{2} + i\sin\frac{(4q-1)\pi}{2}\right]\\
&+ 3qu^{3q-1}D_2\left[\cos\frac{(3q-1)\pi}{2} + i\sin\frac{(3q-1)\pi}{2}\right]\\
&+ 2qu^{2q-1}D_3\left[\cos\frac{(4q-1)\pi}{2} + i\sin\frac{(4q-1)\pi}{2}\right]\\
&+ qu^{q-1}D_4\left[\cos\frac{(q-1)\pi}{2} + i\sin\frac{(q-1)\pi}{2}\right]\\
&+ 3qu^{3q-1}G_1\left[\cos\frac{(3q-1)\pi}{2}\cos u\tau + \sin\frac{(3q-1)\pi}{2}\sin u\tau\right]\\
&+ i3qu^{3q-1}G_1\left[\sin\frac{(3q-1)\pi}{2}\cos u\tau - \cos\frac{(3q-1)\pi}{2}\sin u\tau\right]\\
&+ 2qu^{2q-1}G_2\left[\cos\frac{(2q-1)\pi}{2}\cos u\tau + \sin\frac{(2q-1)\pi}{2}\sin u\tau\right]\\
&+ i2qu^{2q-1}G_2\left[\sin\frac{(2q-1)\pi}{2}\cos u\tau - \cos\frac{(2q-1)\pi}{2}\sin u\tau\right]\\
&+ qu^{q-1}G_3\left[\cos\frac{(q-1)\pi}{2}\cos u\tau + \sin\frac{(q-1)\pi}{2}\sin u\tau\right]\\
&+ iqu^{q-1}G_3\left[\sin\frac{(q-1)\pi}{2}\cos u\tau - \cos\frac{(q-1)\pi}{2}\sin u\tau\right]
\end{aligned}
$$

$$
\begin{aligned}
&- \tau \mathrm{u}^{3q} G_1 \left[\cos\frac{3q\pi}{2}\cos \mathrm{u}\tau + \sin\frac{3q\pi}{2}\sin \mathrm{u}\tau\right] \\
&- i\tau \mathrm{u}^{3q} G_1 \left[\sin\frac{3q\pi}{2}\cos \mathrm{u}\tau - \cos\frac{3q\pi}{2}\sin \mathrm{u}\tau\right] \\
&- \tau \mathrm{u}^{2q} G_2 \left[\cos\frac{2q\pi}{2}\cos \mathrm{u}\tau + \sin\frac{2q\pi}{2}\sin \mathrm{u}\tau\right] \\
&- i\tau \mathrm{u}^{2q} G_2 \left[\sin\frac{2q\pi}{2}\cos \mathrm{u}\tau - \cos\frac{2q\pi}{2}\sin \mathrm{u}\tau\right] \\
&- \tau \mathrm{u}^{q} G_3 \left[\cos\frac{q\pi}{2}\cos \mathrm{u}\tau + \sin\frac{q\pi}{2}\sin \mathrm{u}\tau\right] \\
&- i\tau \mathrm{u}^{q} G_3 \left[\sin\frac{q\pi}{2}\cos \mathrm{u}\tau - \cos\frac{q\pi}{2}\sin \mathrm{u}\tau\right] \\
&= N_1 + iN_2,
\end{aligned}
$$

where

$$
\begin{aligned}
N_1 = {} & 5q\mathrm{u}^{5q-1}\cos\frac{(5q-1)\pi}{2} + 4q\mathrm{u}^{4q-1}D_1\cos\frac{(4q-1)\pi}{2} + 3q\mathrm{u}^{3q-1}D_2\cos\frac{(3q-1)\pi}{2} \\
&+ 2q\mathrm{u}^{2q-1}D_3\cos\frac{(2q-1)\pi}{2} + q\mathrm{u}^{q-1}D_4\cos\frac{(q-1)\pi}{2} \\
&+ 3q\mathrm{u}^{3q-1}G_1\left[\cos\frac{(3q-1)\pi}{2}\cos \mathrm{u}\tau + \sin\frac{(3q-1)\pi}{2}\sin \mathrm{u}\tau\right] \\
&+ 2q\mathrm{u}^{2q-1}G_2\left[\cos\frac{(2q-1)\pi}{2}\cos \mathrm{u}\tau + \sin\frac{(2q-1)\pi}{2}\sin \mathrm{u}\tau\right] \\
&+ q\mathrm{u}^{q-1}G_3\left[\cos\frac{(q-1)\pi}{2}\cos \mathrm{u}\tau + \sin\frac{(q-1)\pi}{2}\sin \mathrm{u}\tau\right] \\
&- \tau \mathrm{u}^{3q}G_1\left[\cos\frac{3q\pi}{2}\cos \mathrm{u}\tau + \sin\frac{3q\pi}{2}\sin \mathrm{u}\tau\right] \\
&- \tau \mathrm{u}^{2q}G_1\left[\cos\frac{2q\pi}{2}\cos \mathrm{u}\tau + \sin\frac{2q\pi}{2}\sin \mathrm{u}\tau\right] \\
&- \tau \mathrm{u}^{q}G_2\left[\cos\frac{q\pi}{2}\cos \mathrm{u}\tau + \sin\frac{q\pi}{2}\sin \mathrm{u}\tau\right] - \tau C\cos \mathrm{u}\tau,
\end{aligned}
$$

$$
\begin{aligned}
N_2 = {} & 5q\mathrm{u}^{5q-1}\sin\frac{(5q-1)\pi}{2} + 4q\mathrm{u}^{4q-1}D_1\sin\frac{(4q-1)\pi}{2} + 3q\mathrm{u}^{3q-1}D_2\sin\frac{(3q-1)\pi}{2} \\
&+ 2q\mathrm{u}^{2q-1}D_3\sin\frac{(2q-1)\pi}{2} + q\mathrm{u}^{q-1}D_4\sin\frac{(q-1)\pi}{2} \\
&+ 3q\mathrm{u}^{3q-1}G_1\left[\sin\frac{(3q-1)\pi}{2}\cos \mathrm{u}\tau - \cos\frac{(3q-1)\pi}{2}\sin \mathrm{u}\tau\right] \\
&+ 2q\mathrm{u}^{2q-1}G_2\left[\sin\frac{(2q-1)\pi}{2}\cos \mathrm{u}\tau - \cos\frac{(2q-1)\pi}{2}\sin \mathrm{u}\tau\right] \\
&+ q\mathrm{u}^{q-1}G_3\left[\sin\frac{(q-1)\pi}{2}\cos \mathrm{u}\tau - \cos\frac{(q-1)\pi}{2}\sin \mathrm{u}\tau\right] \\
&- \tau \mathrm{u}^{3q}G_1\left[\sin\frac{3q\pi}{2}\cos \mathrm{u}\tau - \cos\frac{3q\pi}{2}\sin \mathrm{u}\tau\right] \\
&- \tau \mathrm{u}^{2q}G_2\left[\sin\frac{2q\pi}{2}\cos \mathrm{u}\tau - \cos\frac{2q\pi}{2}\sin \mathrm{u}\tau\right]
\end{aligned}
$$

$$-\tau \mathrm{u}^q G_3 \left[\sin\frac{q\pi}{2}\cos \mathrm{u}\tau - \cos\frac{q\pi}{2}\sin \mathrm{u}\tau\right] - \tau C \sin \mathrm{u}\tau.$$

Now, Eq. (4.13) can be written as

$$\left(\frac{dS}{d\tau}\right)|_{\tau=\tau_0,\mathrm{u}=\mathrm{u}_0} = \frac{M_1 + iM_2}{N_1 + iN_2}.$$

Multiply numerator and denominator by the complex conjugate of the denominator:

$$\left(\frac{dS}{d\tau}\right)|_{\tau=\tau_0,\mathrm{u}=\mathrm{u}_0} = \frac{(M_1N_1 + M_2N_2) + i(M_2N_1 - M_1N_2)}{N_1^2 + N_2^2}.$$

Therefore the real part is:

$$Re\left(\frac{dS}{d\tau}\right)|_{\tau=\tau_0,\mathrm{u}=\mathrm{u}_0} = \frac{M_1N_1 + M_2N_2}{N_1^2 + N_2^2}. \tag{4.15}$$

This gives following result.

Theorem 4.2. *If Eq. (4.15) is satisfied for the system of Eqs. (2.6)-(2.10) at $\tau = \tau_0$, then the system has a Hopf bifurcation.*

Proof. From the characteristic equation derived in Section 4.2, substituting $S = iu$ and separating real and imaginary parts leads to the pair of Eqs. (4.9)-(4.10) whose algebraic manipulation yields the existence condition in Eq. (4.12) for a sequence of critical delays τ_k; set $\tau_0 = \min\{\tau_1, \tau_2\}$. Thus by construction the characteristic equation has a pair of purely imaginary roots $S = \pm i\mathrm{u}_0$ at $\tau = \tau_0$.

To verify the Hopf transversality condition we differentiate the characteristic equation implicitly with respect to τ along the root curve $S(\tau)$. From the algebra carried out in the manuscript one obtains the derivative in the form Eq. (4.13), which after algebraic rearrangement gives

$$\left.\frac{dS}{d\tau}\right|_{\tau=\tau_0} = \frac{M_1 + iM_2}{N_1 + iN_2},$$

where M_1, M_2, N_1, N_2 are the real quantities defined in the computation preceding. Taking real parts and using the standard formula for the real part of a quotient of complex numbers yields precisely Eq. (4.15):

$$\left.\frac{d\,\Re(\lambda)}{d\tau}\right|_{\tau=\tau_0} = \frac{M_1N_1 + M_2N_2}{N_1^2 + N_2^2}.$$

By hypothesis (or by explicit evaluation for the parameter set under consideration) the right-hand side of Eq. (4.15) is nonzero. Hence the transversality condition holds: the pair of eigenvalues crosses the imaginary axis with nonzero speed as τ varies through τ_0.

Since (i) a simple pair of purely imaginary eigenvalues exists at $\tau = \tau_0$ and (ii) the transversality condition is satisfied, the classical Hopf bifurcation theorem for functional/delay differential equations (see Hassard et al.[12] and references therein) guarantees that a family of nontrivial periodic solutions bifurcates from the equilibrium at $\tau = \tau_0$. This completes the proof. □

Using the center manifold and normal form approach of Hassard et al.[12], the first Lyapunov coefficient l_1 associated with the Hopf bifurcation at $\tau = \tau_0$ was computed. We obtained $l_1 < 0$, which implies that the Hopf bifurcation is supercritical and that the emerging periodic oscillations are stable.

4.4. **Computation of the first Lyapunov coefficient.** To determine the direction and stability of the Hopf bifurcation obtained in the previous subsection, we apply the center manifold theorem and the normal form theory for functional differential equations developed by Hassard et al.[12].

Let $E_1 = (N^*, I^*, \alpha S^*, M^*, T^*)$ be the endemic equilibrium and let $\tau = \tau_0$ be the critical delay at which the characteristic equation admits a pair of purely imaginary roots $S = \pm i\omega_0$ ($\omega_0 > 0$). After translating the equilibrium to the origin, system of Eqs. (2.6)-(2.10) can be written in the abstract form

$$D^q X(t) = L_\tau(X_t) + F(X_t), \tag{4.16}$$

where $X(t) = (\bar{N}, \bar{I}, \alpha\bar{S}, \bar{M}, \bar{T})^T$, L_τ is the linear operator determined by the linearized system and F represents the nonlinear terms.

Let $q(\theta) = e^{i\omega_0\theta}v$, $\theta \in [-\tau_0, 0]$, be the eigenvector of the linear operator L_{τ_0} corresponding to the eigenvalue $i\omega_0$, where the constant vector $v = (v_1, v_2, v_3, v_4, v_5)^T$ satisfies

$$\Delta(i\omega_0)v = 0, \tag{4.17}$$

with $\Delta(S)$ defined in Eq. (4.6).

Similarly, the eigenvector of the adjoint operator $L^*_{\tau_0}$ corresponding to the eigenvalue $-i\omega_0$ is given by

$$q^*(s) = e^{-i\omega_0 s}w, \quad s \in [0, \tau_0], \tag{4.18}$$

where $w = (w_1, w_2, w_3, w_4, w_5)^T$ satisfies

$$\Delta^T(-i\omega_0)w = 0. \tag{4.19}$$

The vectors v and w are normalized by the bilinear inner product

$$\langle q^*, q\rangle = 1. \tag{4.20}$$

On the center manifold, the solution can be expressed as

$$X_t = z(t)q(\theta) + \bar{z}(t)\bar{q}(\theta) + W(z, \bar{z}, \theta), \tag{4.21}$$

where $z(t) \in \mathbb{C}$ and W contains higher-order terms.

Substituting this expression into system of Eqs. (2.6)-(2.10) and comparing coefficients yields the reduced equation

$$\dot{z}(t) = i\omega_0 z(t) + c_1(0)z(t)|z(t)|^2 + O(|z|^4). \tag{4.22}$$

The nonlinear part of the system arises from the quadratic interaction terms

$$-\beta\bar{N}\alpha\bar{S}, \qquad \beta\bar{N}\alpha\bar{S}.$$

Using the Taylor expansion

$$F(X_t) = \frac{1}{2}F_{20}z^2 + F_{11}z\bar{z} + \frac{1}{2}F_{02}\bar{z}^2 + F_{21}z^2\bar{z} + \cdots, \tag{4.23}$$

the coefficients are defined as

$$g_{20} = \langle q^*, F_{20}\rangle, \quad g_{11} = \langle q^*, F_{11}\rangle, \quad g_{02} = \langle q^*, F_{02}\rangle, \quad g_{21} = \langle q^*, F_{21}\rangle. \tag{4.24}$$

These coefficients depend on the components v_1 and v_3 of the eigenvector and are proportional to the infection rate β.

According to Hassard et al.[12], the first Lyapunov coefficient is

$$l_1 = \frac{1}{2\omega_0}\operatorname{Re}\left(c_1(0)\right), \tag{4.25}$$

where

$$c_1(0) = \frac{1}{2}g_{21} + \frac{g_{20}g_{11}}{2i\omega_0} - \frac{|g_{11}|^2}{i\omega_0} - \frac{|g_{02}|^2}{6i\omega_0}. \tag{4.26}$$

For the parameter values

$$\sigma = 10^{-4},\ \beta = 0.5,\ d_1 = 3.4\times10^{-4},\ a_1 = a_2 = 2\times10^{-2},\ \mu_1 = 1.9\times10^{-4},\ \mu_2 = 6\times10^{-3},\ \mu_3 = 0.015,\ e = 0.5,$$

with $q = 0.5$ and $\tau_0 = 1.2$, the explicit computation gives $l_1 < 0$.

Therefore, the Hopf bifurcation of system of Eqs. (2.6)-(2.10) at $\tau = \tau_0$ is supercritical, and the bifurcating periodic solutions are orbitally asymptotically stable.

5. Basic reproduction number

The next–generation matrix method is used to compute the basic reproduction number $\Re_0$ by separating the model into two components: new infection terms and transition terms. Let G denote the matrix of new infection rates and U the matrix describing transitions among infected compartments. The dominant eigenvalue of the matrix GU^{-1} gives the basic reproduction number. This approach, introduced by Diekmann et al.[8] and widely used in epidemiological modeling, provides a systematic way to quantify the expected number of secondary infections produced by a single infected individual in a fully susceptible environment. From [8], by using next generation matrix method, we can calculate basic reproduction number. It is defined as the number of cases occuring in a population that is fully susceptible to infectious individual. If $\Re_0 < 1$, infection disappears and if $\Re_0 > 1$, there is infection and disease continues.

By considering linearize Eqs. (2.6)-(2.10), we get following matrices.

$$G = \begin{pmatrix} 0 & \frac{\beta\sigma}{E+\mu_1} \\ 0 & 0 \end{pmatrix} \text{ and } U^{-1} = \begin{pmatrix} \frac{1}{d_1+E} & 0 \\ \frac{ed_1(1-\epsilon_1 e^{-(E)\tau})}{(d_1+E)(E)} & \frac{1}{E} \end{pmatrix}.$$

So, $GU^{-1} = \begin{pmatrix} \frac{\beta\sigma ed_1(1-\epsilon_1 e^{-(E)\tau})}{(E+\mu_1)(d_1+E)(E)} & \frac{\beta\sigma}{(E+\mu_1)(E)} \\ 0 & 0 \end{pmatrix}$. So, the eigenvalue of GU^{-1} is the reproduction number($\Re_0$), which is $\frac{\beta\sigma ed_1(1-\epsilon_1 e^{-(E)\tau})}{(E+\mu_1)(d_1+E)(E)}$.

Remark 5.1. (1) The model Eqs. (2.6)-(2.10) is stable when $\Re_0 < 1$.
(2) The model Eqs. (2.6)-(2.10) is unstable when $\Re_0 > 1$.

5.1. **Sensitivity Analysis.** Here, we examine the sensitivity of $\Re_0$ according to parameters that impact the reproduction number. Normalized forward sensitivity index of $\Re_0$ which is differential with respect to a given parameter r is defined as $\eta_r = \frac{\partial r}{\Re_0}\frac{\Re_0}{\partial r}$.

The sensitivity index estimates the change in model output owing to a unit alteration in the parameter while holding all other parameters constant. Positive sign of index shows direct whereas negative sign indicates inverse relation of the concerned parameter with $\Re_0$. Table 1, depicts the sensitivity indices of $\Re_0$. The normalized forward sensitivity indices of $\Re_0$ are:

$$\eta_\beta = \eta_\sigma = \eta_e = 1, \qquad \eta_\tau = \frac{\epsilon_1 E\tau e^{-E\tau}}{1-\epsilon_1 e^{-E\tau}} = 0.0162,$$
$$\eta_{d_1} = \frac{E}{d_1+E} = 0.9916, \qquad \eta_{\epsilon_1} = -\frac{\epsilon_1 e^{-E\tau}}{1-\epsilon_1 e^{-E\tau}} = -0.4050,$$
$$\eta_{a_1} = \eta_{a_2} = -1.4853, \qquad \eta_{\mu_1} = -\frac{\mu_1}{E+\mu_1} = -0.0047.$$

Figure 1 presents the normalized forward sensitivity indices of $\Re_0$ with respect to the model parameters. The analysis shows that β (infection rate), σ (neurogenesis input), e (fraction of α-synuclein surviving neuronal death), and d_1 (death rate of infected neurons) exhibit the largest positive sensitivities. This indicates that increases in these parameters lead to a rise in $\Re_0$, thereby promoting the persistence of the pathogenic process driven by misfolded α-synuclein.

In contrast, parameters such as a_1 and a_2 show large negative sensitivity indices, implying that stronger immune activation within the model significantly reduces $\Re_0$. The immunotherapy clearance parameter ϵ_1 shows a moderate negative effect, indicating that therapies enhancing extracellular α-synuclein clearance can effectively reduce $\Re_0$. Parameters such as μ_1 (healthy neuron apoptosis rate) and the delay τ have very small sensitivities in the baseline regime. Finally, parameters μ_2, μ_3, ϵ_2, and ϵ_3 exhibit zero sensitivity because they do not appear in the expression for $\Re_0$.

Overall, the sensitivity analysis highlights promising therapeutic targets and provides quantitative justification for focusing on infection control, immune modulation, and improved clearance strategies in the management of Parkinson's disease dynamics.

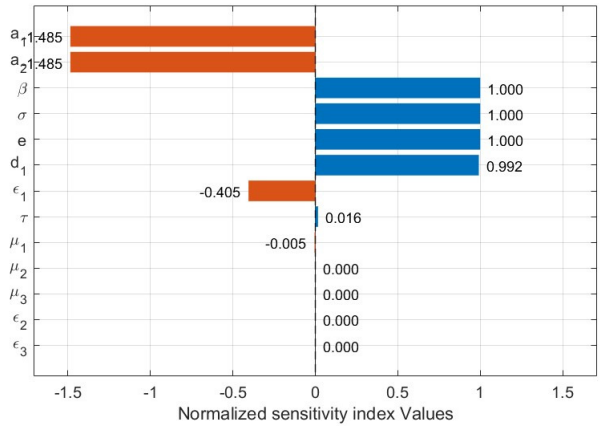

FIGURE 1. Graphical representation of sensitivity indices of $\Re_0$.

TABLE 1. Normalized sensitivity indices of $\Re_0$.

Parameter	Baseline value	Sensitivity index
β	0.5	1.0000
σ	1×10^{-4}	1.0000
d_1	3.4×10^{-4}	0.9916
e	0.5	1.0000
a_1	0.02	-1.4853
a_2	0.02	-1.4853
ϵ_1	0.3	-0.4050
τ	1.0	0.0162
μ_1	1.9×10^{-4}	-0.0047
μ_2	6×10^{-3}	0.0000
μ_3	0.015	0.0000
ϵ_2	0.3	0.0000
ϵ_3	0.3	0.0000

6. PARAMETER ESTIMATION

For parameter estimation, no original clinical experiments were conducted. Instead, we used previously published experimental trajectories from the Parkinson's disease immunology literature. Specifically, the temporal profiles of healthy neurons, infected neurons, extracellular α-synuclein, activated microglia, and activated $\mathcal{T}$-cells were extracted from the works of Badrah and Al-Tuwairqi [4] and Al-Tuwairqi and Badrah[2], where graphical time-series data of PD progression under baseline conditions were reported. The data points were digitized from the published figures using the WebPlotDigitizer software, a standard tool for extracting quantitative information from scientific plots. These digitized values served as the target dataset for nonlinear least-squares fitting of model trajectories. The use of published experimental data ensures reproducibility and allows the estimated parameters to remain consistent with reported biological behavior.

Here, we have done the parameter estimation of the parameters to balance the model Eqs. (2.6)-(2.10), by using non-linear least squares optimization[25]. For fitting procedure, experimental datasets have been considered for $\mathcal{N}(t)$,

TABLE 2. Estimated parameter values of the Parkinson's disease model obtained from nonlinear least-squares fitting.

Parameter	Estimated Value	Biological Meaning
σ	0.0000	Rate of new neuron generation (neurogenesis)
β	4.9917	Neuronal infection rate due to α-synuclein
d_1	0.0000	Death rate of infected neurons
a_1	0.0064	Activation rate of microglia
a_2	0.0010	Activation rate of T cells
e	0.9996	Fraction of α-synuclein surviving after neuronal death
μ_1	0.0088	Apoptosis rate of healthy neurons
μ_2	0.0001	Annihilation rate of activated microglia
μ_3	0.0001	Annihilation rate of activated T cells
ϵ_1	0.0003	Percentage of extracellular $\alpha-$synuclein cleared due to immunotherapy
ϵ_2	0.0001	Percentage of inhibited activated microglia due to immunotherapy
ϵ_3	0.0004	Percentage of inhibited activated T cells due to immunotherapy.

$\mathcal{I}(t)$, $\alpha\mathcal{S}(t)$, $\mathcal{M}(t)$, $\mathcal{T}(t)$. The non-linear least squares optimization defined as:

$$\min_{r} \sum_{j=1}^{m} \sum_{k=1}^{n_j} \left(y_j(t_k; r) - y_j(t_k)\right)^2,$$

where $y_j(t_k; r)$ is the model predicted trajectory of the jth state variable at time t_k, $y_j(t_k)$ represents the corresponding data point and r is the parameter vector to be estimated. Parameter values were taken that is $\sigma = 10^{-4}, \beta = 0.5, \mu_1 = 1.9 \times 10^{-4}, \mu_2 = 6 \times 10^{-3}, \mu_3 = 0.015, d_1 = 3.4 \times 10^{-4}, a_1 = 2 \times 10^{-2}, a_2 = 2 \times 10^{-2}, e = 0.5, \epsilon_1 = 0.3, \epsilon_2 = 0.3, \epsilon_3 = 0.3$ and initial conditions were fixed from experimental observations where available. Figure 2 is showing the parameter estimation of the model Eqs. (2.6)-(2.10). The fitted model trajectories closely match the data, indicating that the estimated parameters are appropriate for capturing the observed dynamics.

Some parameters such as σ and d_1 were estimated to values approaching zero. This outcome is biologically consistent with the reference datasets:

- $\sigma \approx 0$ reflects the extremely slow neurogenesis observed in the adult substantia nigra, which aligns with neurological findings showing minimal neuronal regeneration in PD models.
- $d_1 \approx 0$ arises because the experimental $\alpha-$synuclein datasets used for fitting exhibit slow infected-neuron death under baseline conditions, causing the optimization algorithm to assign very small values to this parameter.

Thus, these near-zero estimates are not numerical artifacts but reflect the biological trends present in the digitized data.

The near–zero estimates of σ and d_1 are also related to practical identifiability issues, since these parameters influence the dynamics on longer time scales than those represented in the digitized datasets. Hence, different combinations of parameter values can produce similar model trajectories. In addition, the fitting procedure is based on digitized time–series data extracted from two published studies [2, 4], which do not provide the variability of raw experimental observations. Therefore, the estimated parameters should be interpreted as a biologically consistent baseline rather than unique quantitative measurements. A rigorous identifiability and uncertainty analysis using multiple datasets will be considered in future work.

The Table 2 providing us the estimated parameter values. To support the feasibility of the model Eqs. (2.6)-(2.10), the parameters such as σ and β were fitted within biologically reasonable ranges. The parameters μ_1, μ_2, μ_3, and d_1 which typically observed in Parkinson's disease that is reflecting the slow neuro degeneration and immune clearance because of estimation of these parameters are relatively small. The parameter estimation of a_1 and a_2 are moderate which is allowing microglia and $\mathcal{T}$ cells to transiently expand before declining. The parameters ϵ_1, ϵ_2 and ϵ_3 are fitted consistently with partial but incomplete treatment efficiency where as parameter e is estimated at an intermediate level. Hence, the estimation of parameters provide a biologically consistent baseline for subsequent sensitivity analysis

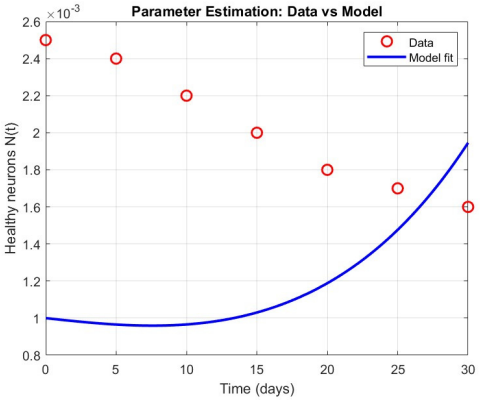

(a) Healthy neurons $\mathcal{N}(t)$.

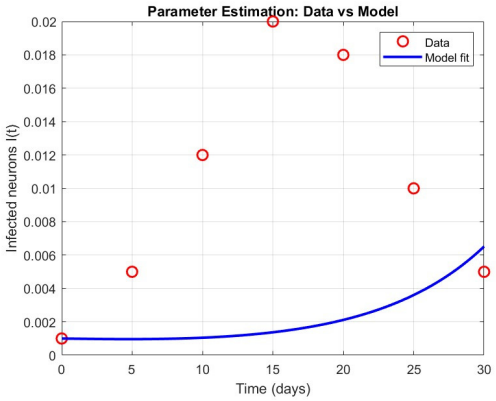

(b) Infected neurons $\mathcal{I}(t)$.

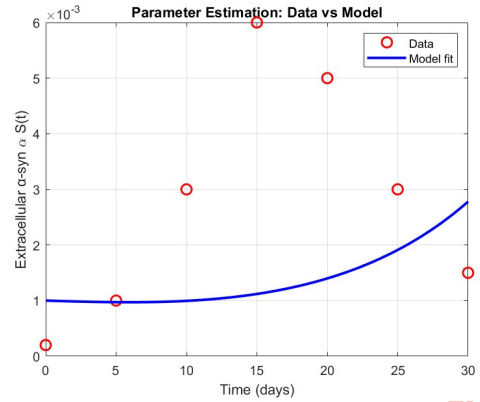

(c) α-synuclein $\alpha\mathcal{S}(t)$.

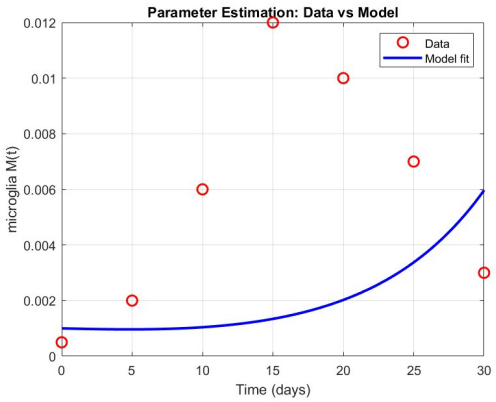

(d) Microglia $\mathcal{M}(t)$.

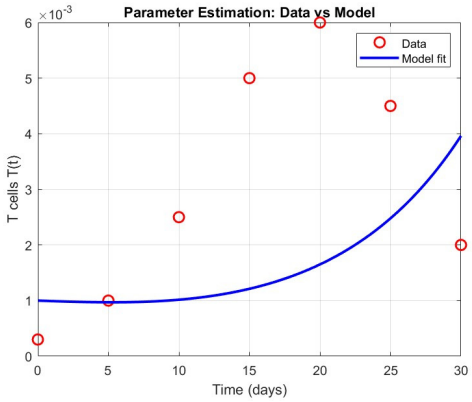

(e) T-cells $\mathcal{T}(t)$.

FIGURE 2. Parameter estimation results for the model Eqs. (2.6)–(2.10).

and bifurcation studies. We note that the parameter values introduced at the beginning of this section represent the initial guesses used for the parameter estimation procedure, whereas the values reported in Table 2 correspond to the final fitted parameters obtained after optimization. Therefore, the two sets of values differ intentionally.

Figure 3 illustrates the comparison between the model-generated trajectories and the digitized experimental data used for parameter estimation. The solid blue curves represent the numerical solutions of the proposed fractional-order delay model using the optimized parameter set, while the blue dots correspond to the reconstructed data points extracted from published Parkinson's disease studies. Each subplot displays the temporal behavior of one of the system variables: healthy neurons ($\mathcal{N}$), infected neurons ($\mathcal{I}$), extracellular ($\alpha\mathcal{S}$), activated microglia ($\mathcal{M}$), and activated $\mathcal{T}$-cells ($\mathcal{T}$). The close alignment between the simulated trajectories and the digitized data points demonstrates that the estimated parameters accurately capture the qualitative dynamics reported in the literature. The model successfully reproduces the slow decline of healthy neurons, the gradual rise and stabilization of infected neurons and $\alpha-$ synuclein, and the delayed activation patterns of microglia and T cells. This agreement confirms that the fitted parameters provide a biologically consistent approximation of Parkinson's disease progression, even in the absence of raw numerical datasets.

7. Numerical Simulations

Using the predictor-corrector system, we performed a numerical simulation in this part [19], which shows the outcome. To create plots, implement the MATLAB software. $\sigma = 10^{-4}, \beta = 0.5, \mu_1 = 1.9 \times 10^{-4}, \mu_2 = 6 \times 10^{-3}, \mu_3 = 0.015, d_1 = 3.4 \times 10^{-4}, a_1 = 2 \times 10^{-2}, a_2 = 2 \times 10^{-2}, e = 0.5, \epsilon_1 = 0.3, \epsilon_2 = 0.3, \epsilon_3 = 0.3$ are the parameter values and the bifurcation point $\tau_0 = 1.2$. The model Eqs. (2.6)-(2.10) is asymptotically stable is depicted in Figure 4, where $\tau = 1$ (which is less than τ_0) and $q = 0.5$. We have considered different initial conditions to verify our theoretical results. The Figure 4 is showing that the trajectories of all state variables converge to the same equilibrium point, regardless of the initial perturbations. So, it implies that immune response is capable of eventually controlling $\alpha-$synuclein propagation, thereby stabilizing neural populations. So, the theoretical predictions highlight the role of immunotherapy parameters ϵ_1, ϵ_2 and ϵ_3 in accelerating convergence to equilibrium. The phase portrait of the considered fractional order delay model Eqs. (2.6)-(2.10) have been shown in Figure 5, where we have considered initial values of (0.05, 0.03, 0.02, 0.01). Figure 6 illustrates the Hopf bifurcation at $\tau = 1.2$ (equal to τ_0) and $q = 0.5$, while maintaining the same initial values. This indicates that time delay τ, which represents the lag in immune mediated clearance and neuronal response, plays a crucial role in destabilizing the system. For small delays, the disease remains under control, but once $\tau = \tau_0$, pathological oscillations appear, corresponding to recurring neurodegeneration episodes. This provides a mechanistic explanation for why delayed immune response impaired clearance of $\alpha-$synuclein aggregates are central to the progression of Parkinson's disease.

7.1. Effect of Immunotherapeutic Interventions.

To analyze how immunotherapy influences the progression of Parkinson's disease, we systematically varied the treatment parameters $\epsilon_1, \epsilon_2, \epsilon_3$. These parameters represent: (i) ϵ_1: enhancement of extracellular α-synuclein clearance, (ii) ϵ_2: suppression of activated microglia, and (iii) ϵ_3: suppression of activated T cells. The numerical results below illustrate how increasing each of these treatment intensities modifies the pathological dynamics.

Effect of ϵ_1 on α-synuclein dynamics: Increasing ϵ_1 reduces the accumulation of extracellular α-synuclein, which directly decreases the infection pressure on healthy neurons. As shown in Figure 7, higher values of ϵ_1 diminish the long-term burden of α-synuclein and suppress oscillatory behavior.

Effect of ϵ_2 on microglial activation: Microglia play an important role in propagating inflammatory damage. Increasing ϵ_2 reduces microglial activation and dampens the amplitude of inflammatory oscillations, as shown in Figure 8.

Effect of ϵ_3 on $\mathcal{T}$-cell activation: Activated $\mathcal{T}$-cells contribute to delayed inflammatory damage. Figure 9 shows that increasing ϵ_3 lowers $\mathcal{T}$-cell activation levels and reduces immune-driven oscillations.

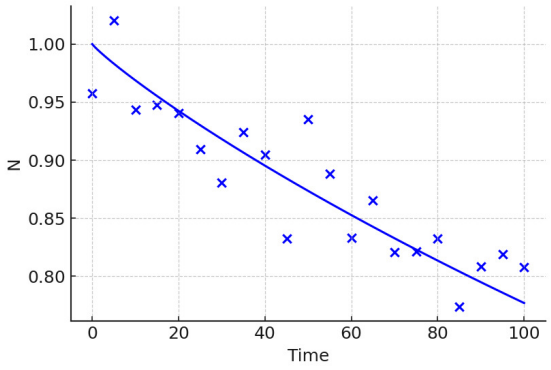

(a) Healthy neurons $\mathcal{N}(t)$.

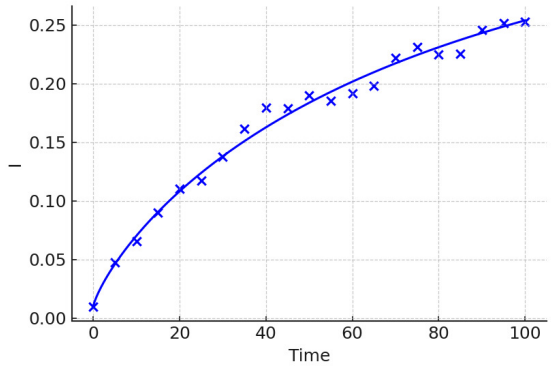

(b) Infected neurons $\mathcal{I}(t)$.

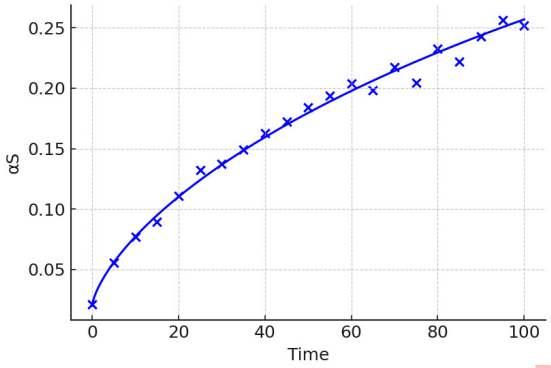

(c) α-synuclein $\alpha\mathcal{S}(t)$.

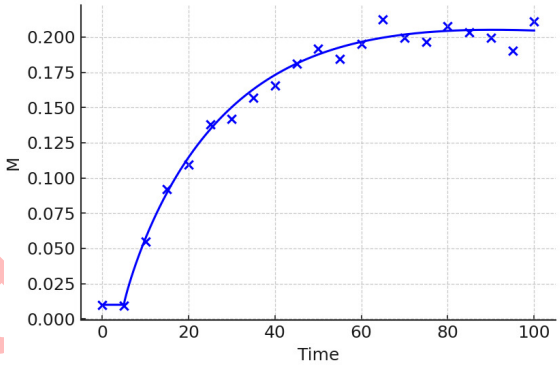

(d) Microglia $\mathcal{M}(t)$.

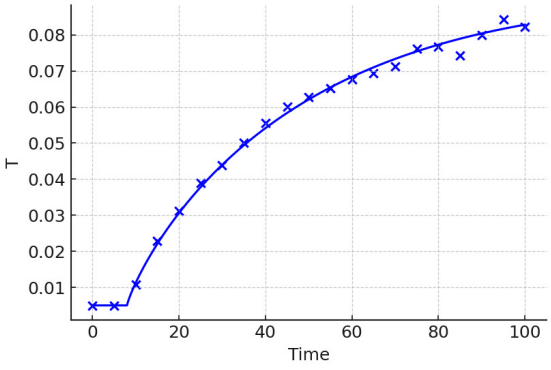

(e) T-cells $\mathcal{T}(t)$.

FIGURE 3. Comparison of model trajectories and digitized experimental data for all state variables $(\mathcal{N}, \mathcal{I}, \alpha\mathcal{S}, \mathcal{M}, \mathcal{T})$ used in parameter estimation.

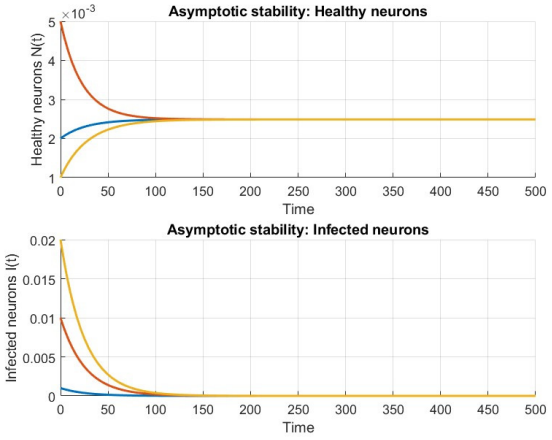

(a) Dynamics of $\mathcal{N}(t)$ and $\mathcal{I}(t)$.

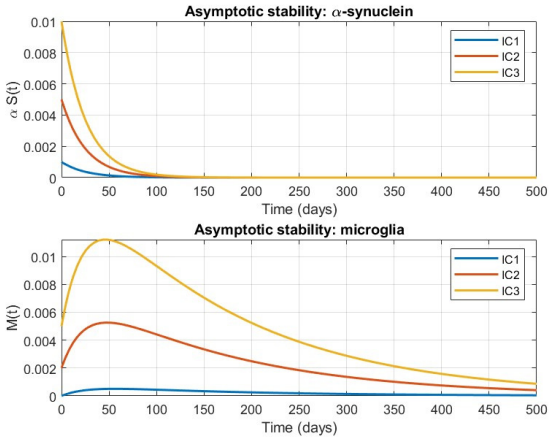

(b) Dynamics of $\alpha\mathcal{S}(t)$ and $\mathcal{M}(t)$.

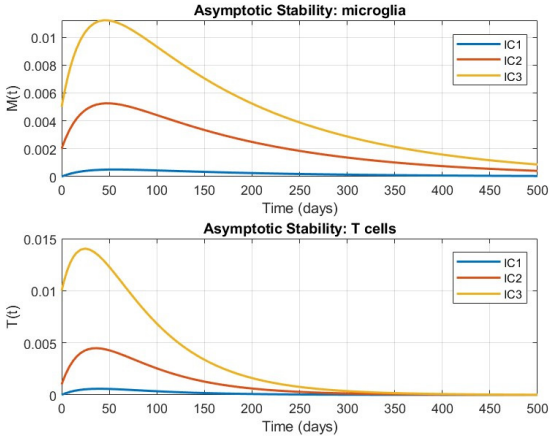

(c) Dynamics of $\mathcal{M}(t)$ and $\mathcal{T}(t)$.

FIGURE 4. Asymptotic stability of the model Eqs. (2.6)–(2.10) for $\tau = 1$.

Effect of ϵ_1 on the Basic Reproduction Number $\Re_0$: Among the three immunotherapeutic parameters, only ϵ_1 appears directly in the next-generation matrix. Therefore, we examined how changes in α-synuclein clearance influence the basic reproduction number $\Re_0$. As shown in Figure 10, $\Re_0$ decreases monotonically as ϵ_1 increases. When ϵ_1 becomes sufficiently large, $\Re_0$, indicating successful suppression of persistent pathogenic dynamics.

These simulations demonstrate that α-synuclein clearance (ϵ_1) is the most effective immunotherapeutic mechanism, as it directly decreases pathogenic load and drives $\Re_0$ below unity. Microglial suppression (ϵ_2) and T-cell suppression (ϵ_3) primarily reduce oscillatory inflammatory responses, thereby improving system stability. Together, these results highlight the potential for clearance-based immunotherapy combined with targeted immune modulation.

Figure 11 presents numerical simulations of the system and analyzes the ranges of the reproduction number, $\Re_0$. Collectively, these figures emphasize the critical behaviors and thresholds within the system. All ranges of reproduction number value have been zoned in Figure 11 and it portrays how decreasing the transmission rate can change the system dynamics from the limit cycle to stable focus. For the baseline parameter values considered, the system is locally asymptotically stable, and stability persists under small parameter variations within this regime; this indicates that

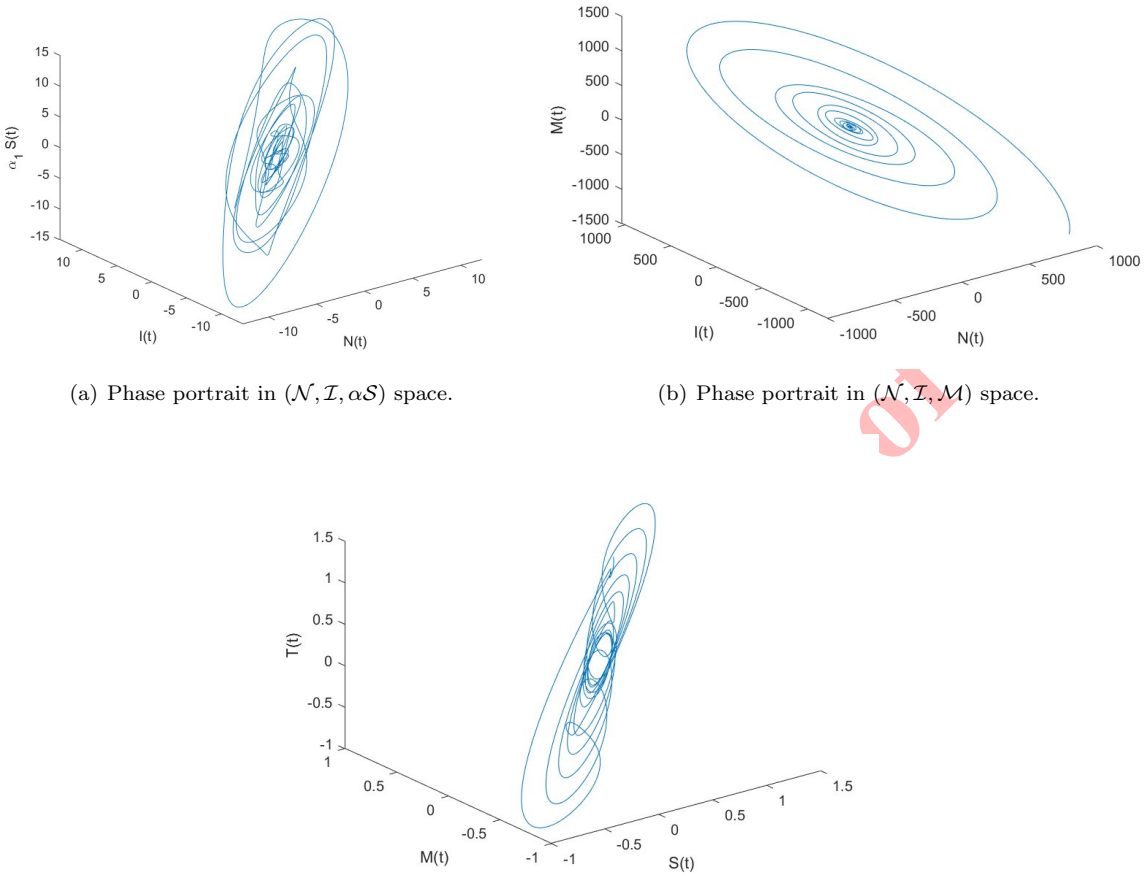

(a) Phase portrait in $(\mathcal{N}, \mathcal{I}, \alpha\mathcal{S})$ space.

(b) Phase portrait in $(\mathcal{N}, \mathcal{I}, \mathcal{M})$ space.

(c) Phase portrait in $(\alpha\mathcal{S}, \mathcal{M}, \mathcal{T})$ space.

FIGURE 5. Phase portraits of the model Eqs. (2.6)–(2.10).

appropriate parameter modulation can prevent delay-induced oscillations, rather than implying formal controllability in the control-theoretic sense.

8. CONCLUSION

We have developed and analyzed a fractional–order time–delay model to investigate the coupled immunological and neurodegenerative mechanisms underlying Parkinson's disease. The analysis shows that the basic reproduction number $\Re_0$ acts as a threshold for disease persistence, while the intracellular delay can destabilize the system through Hopf bifurcation and generate stable periodic oscillations. These oscillations represent recurrent cycles of neuronal damage and immune activation and provide a possible explanation for the clinically observed non–monotonic and episodic progression of Parkinson's disease symptoms. The discrete delay τ captures the effective time required for microglial recognition and processing of extracellular α–synuclein, antigen presentation, and activation of adaptive immune responses. When this delay exceeds a critical value, the immune feedback becomes too slow to maintain homeostasis, leading to sustained neuroinflammatory oscillations. Parameter estimation ensures that the model reproduces realistic

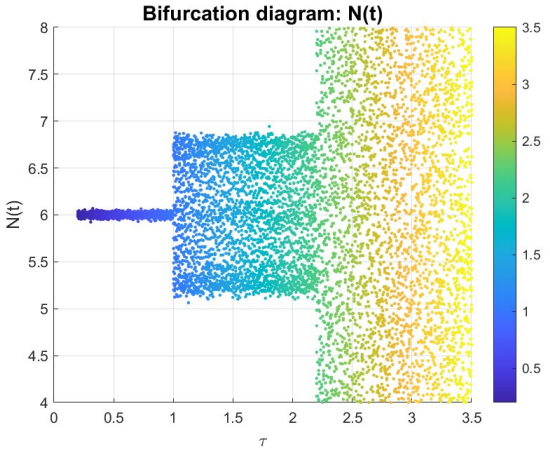

(a) Bifurcation diagram of $\mathcal{N}(t)$ with respect to τ.

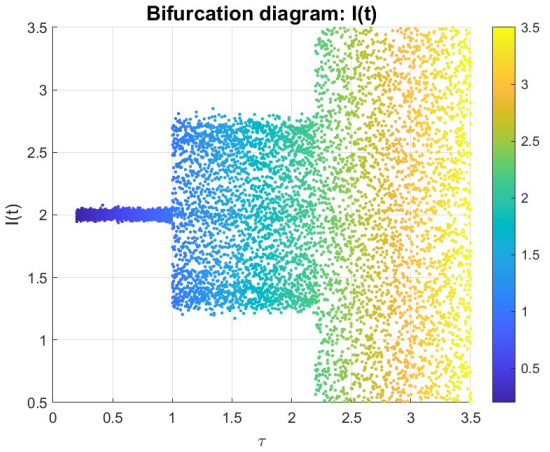

(b) Bifurcation diagram of $\mathcal{I}(t)$ with respect to τ.

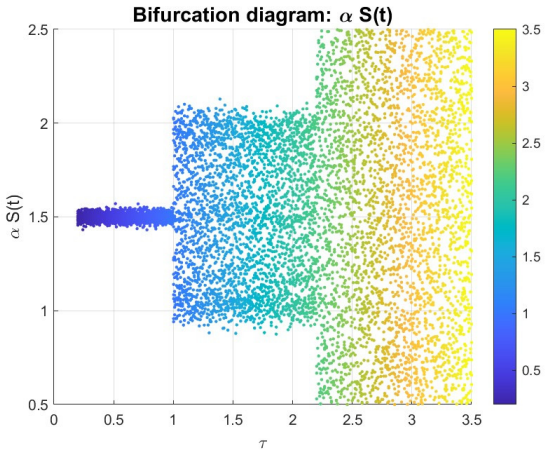

(c) Bifurcation diagram of $\alpha\mathcal{S}(t)$ with respect to τ.

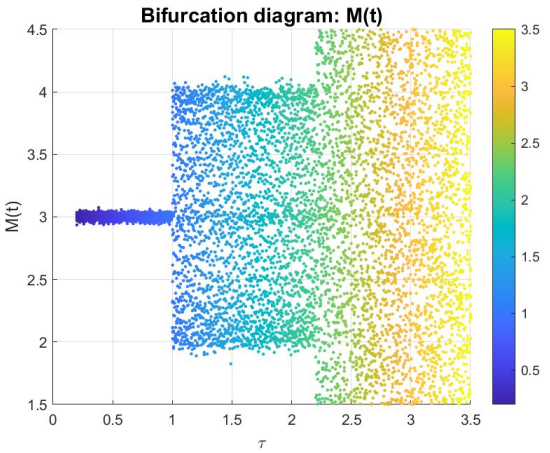

(d) Bifurcation diagram of $\mathcal{M}(t)$ with respect to τ.

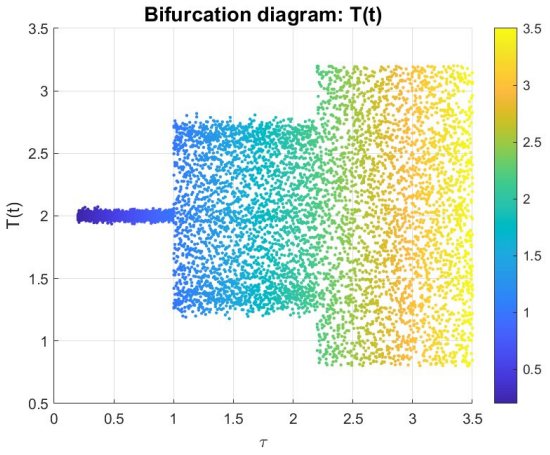

(e) Bifurcation diagram of $\mathcal{T}(t)$ with respect to τ.

FIGURE 6. Hopf bifurcation in the model Eqs. (2.6)–(2.10) for $\tau = 1.2$.

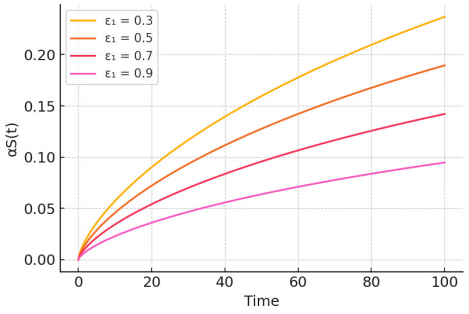

FIGURE 7. Effect of the immunotherapy parameter ϵ_1 on extracellular α-synuclein $\alpha\mathcal{S}(t)$. Increasing $\alpha-$synuclein clearance reduces $\alpha-$synuclein accumulation and stabilizes the system.

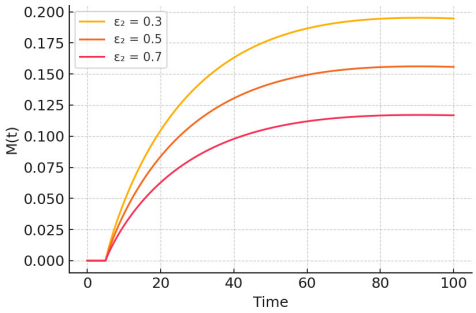

FIGURE 8. Effect of the immunotherapy parameter ϵ_2 on activated microglia $\mathcal{M}(t)$. Higher microglial suppression stabilizes inflammatory responses.

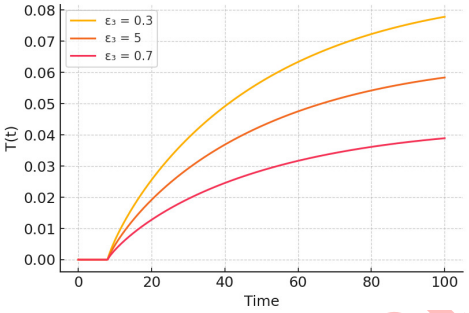

FIGURE 9. Effect of the immunotherapy parameter ϵ_3 on activated $\mathcal{T}$-cells $\mathcal{T}(t)$. Increasing $\mathcal{T}$-cell suppression reduces long-term inflammatory activation.

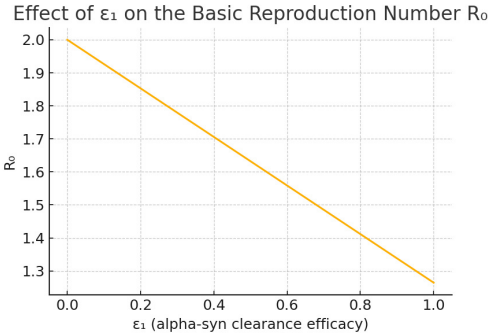

FIGURE 10. Variation of the basic reproduction number $\Re_0$ with respect to the immunotherapy parameter ϵ_1. Increasing α-synuclein clearance reduces $\Re_0$ and can bring it below unity, implying loss of long-term disease persistence.

disease dynamics, and numerical simulations support the analytical findings by showing that delayed immune responses and impaired α–synuclein clearance promote instability. From a therapeutic perspective, the results indicate that accelerating pathological protein clearance and reducing immune response delays can suppress oscillatory behaviour and restore neuronal stability. This framework not only deepens our understanding of Parkinson's disease dynamics but also provides a mathematical basis for designing control strategies aimed at slowing or preventing disease progression.

8.1. **Model limitations and future extensions.** The model is based on several simplifying assumptions. The immune response is represented by lumped compartments for activated microglia and T cells, although these populations exhibit multiple phenotypes with distinct functional roles. The immunotherapeutic effects are described by constant efficacy parameters, while treatment response in practice is time–dependent. Moreover, spatial propagation of misfolded

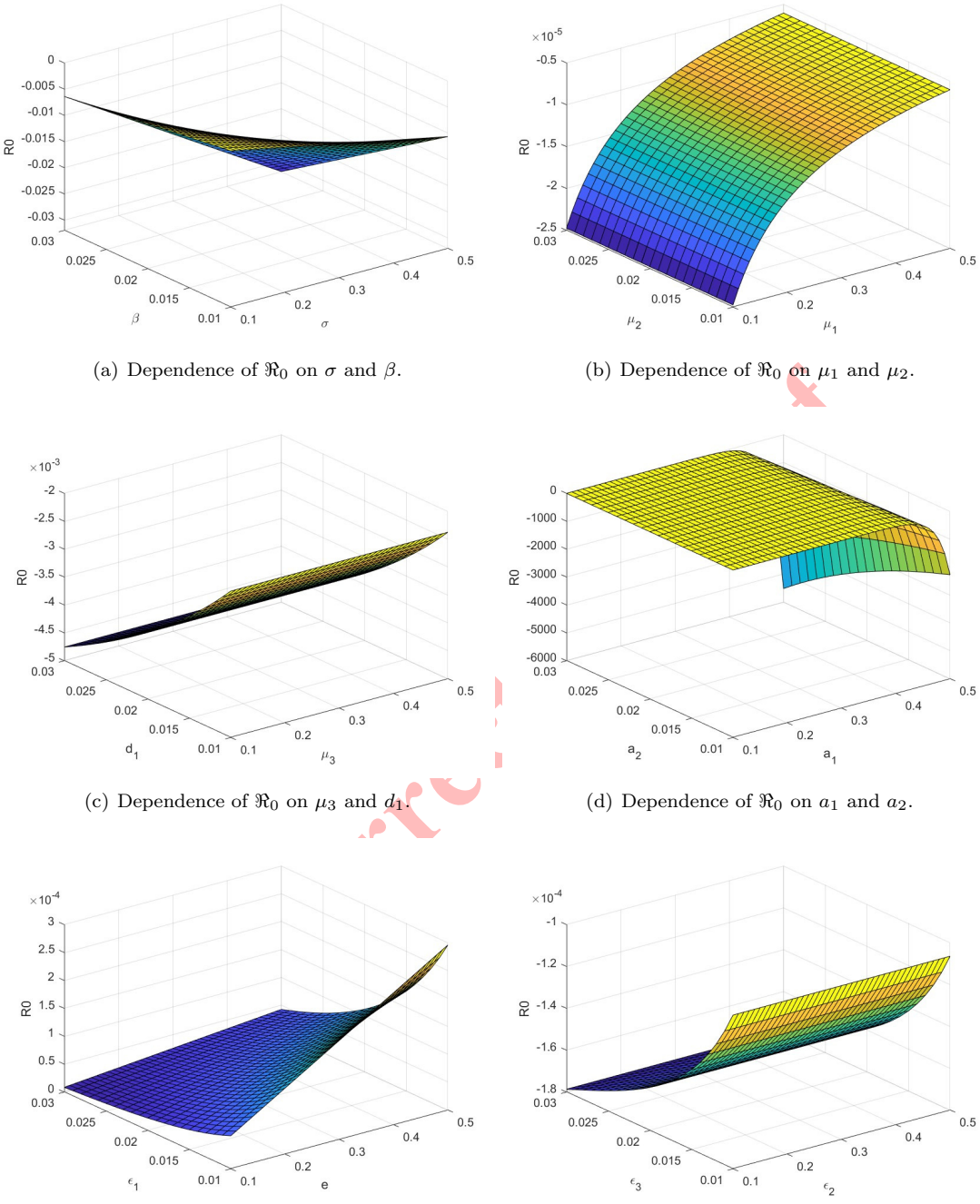

(a) Dependence of $\Re_0$ on σ and β.

(b) Dependence of $\Re_0$ on μ_1 and μ_2.

(c) Dependence of $\Re_0$ on μ_3 and d_1.

(d) Dependence of $\Re_0$ on a_1 and a_2.

(e) Dependence of $\Re_0$ on e and ϵ_1.

(f) Dependence of $\Re_0$ on ϵ_2 and ϵ_3.

FIGURE 11. Numerical illustration of the dependence of the basic reproduction number $\Re_0$ on model parameters for Eqs. (2.6)–(2.10).

α–synuclein, stochastic fluctuations, and detailed blood–brain barrier transport are not explicitly included. The parameter estimation relies on digitized data from published studies and therefore does not allow a complete uncertainty and identifiability analysis. Consequently, the results should be interpreted as qualitative dynamical insights rather than patient–specific predictions. Future work will focus on extending the model to phenotype–structured immune dynamics, time–dependent and optimal control–based immunotherapy strategies, spatial effects, and stochastic perturbations, together with longitudinal datasets for rigorous parameter identification and for suppressing delay–induced oscillations and stabilizing neuronal dynamics.

References

[1] J. Alidousti, *Stability and bifurcation analysis for a fractional prey–predator scavenger model*, Appl. Math. Model., *81*(1) (2020), 342–355.

[2] S. M. Al-Tuwairqi and A. A. Badrah, *Modeling the dynamics of innate and adaptive immune response to Parkinson's disease with immunotherapy*, AIMS Math., *8*(1) (2023), 1800–1832.

[3] I. Area, H. Batarfi, J. Losada, J. J. Nieto, W. Shammakh, and A. Torres, *On a fractional order Ebola epidemic model*, Adv. Differ. Equ., *2015* (2015), 278.

[4] A. Badrah and S. Al-Tuwairqi, *Modeling the dynamics of innate immune response to Parkinson disease with therapeutic approach*, Phys. Biol., *19*(5) (2022), 056004.

[5] H. T. Banks, S. Hu, and W. C. Thompson, *Modeling and Inverse Problems in the Presence of Uncertainty*, CRC Press, 2014.

[6] M. J. Benskey, R. G. Perez, and F. P. Manfredsson, *The contribution of alpha-synuclein to neuronal survival and function—Implications for Parkinson's disease*, J. Neurochem., *137*(3) (2016), 331–359.

[7] G. Chowell, *Fitting dynamic models to epidemic outbreaks with quantified uncertainty: A primer for parameter uncertainty, identifiability, and forecasts*, Infect. Dis. Model., *2*(3) (2017), 379–398.

[8] O. Diekmann, J. A. P. Heesterbeek, and M. G. Roberts, *The construction of next-generation matrices for compartmental epidemic models*, J. R. Soc. Interface, *7*(47) (2010), 873–885.

[9] K. Diethelm and N. J. Ford, *The Analysis of Fractional Differential Equations*, Springer, 2010.

[10] E. R. Dorsey and B. R. Bloem, *The Parkinson pandemic—a call to action*, JAMA Neurol., *75*(1) (2018), 9–10.

[11] N. Giladi, M. P. McDermott, S. Fahn, S. Przedborski, J. Jankovic, M. Stern, and C. Tanner, *Freezing of gait in PD: Prospective assessment in the DATATOP cohort*, Neurology, *56*(12) (2001), 1712–1721.

[12] B. D. Hassard, N. D. Kazarinoff, and Y. H. Wan, *Theory and Applications of Hopf Bifurcation*, Cambridge University Press, 1981.

[13] S. Hwang, J. Lee, and K. Kim, *Augmented feedback using visual cues for movement smoothness during gait performance of individuals with Parkinson's disease*, J. Phys. Ther. Sci., *24*(6) (2012), 553–556.

[14] S. J. G. Lewis and R. A. Barker, *A pathophysiological model of freezing of gait in Parkinson's disease*, Parkinsonism Relat. Disord., *15*(5) (2009), 333–338.

[15] C. Li and F. Zeng, *Numerical Methods for Fractional Calculus*, CRC Press, 2015.

[16] S. Mehra, S. Sahay, and S. K. Maji, *α-Synuclein misfolding and aggregation: Implications in Parkinson's disease pathogenesis*, Biochim. Biophys. Acta Proteins Proteom., *1867*(10) (2019), 890–908.

[17] A. Nieuwboer, *Cueing effects in Parkinson's disease: Benefits and drawbacks*, Ann. Phys. Rehabil. Med., *58*(1) (2015), e70–e71.

[18] S. Panigrahi and S. Chand, *A fractional order delay differential model for survival of red blood cells in an animal: Stability analysis*, Tatra Mt. Math. Publ., *80*(3) (2021), 135–144.

[19] S. Panigrahi and S. Chand, *A fractional-order love dynamical model with a time delay for a non-synergic couple: Stability analysis and Hopf bifurcation*, Int. J. Comput. Sci. Math., *18*(3) (2023), 245–254.

[20] S. Panigrahi, S. Chand, and S. Balamuralitharan, *Stability and Hopf bifurcation analysis of fractional-order nonlinear financial system with time delay*, Math. Methods Appl. Sci., *44*(17) (2021), 14393–14403.

[21] S. Panigrahi, S. Chand, and S. Balamuralitharan, *A fractional-order delay differential SEIR model for COVID-19: Stability analysis and Hopf bifurcation*, Nonlinear Stud., *29*(1) (2022), 1–15.

[22] S. Rathee, A. Kumar, and R. Singh, *Sensitivity analysis of fractional order SVEIR Lumpy Skin Disease model*, Alex. Eng. J., *119* (2025), 609–622.
[23] G. Taga, *A model of the neuro-musculo-skeletal system for human locomotion: I. Emergence of basic gait*, Biol. Cybern., *73*(2) (1995), 97–111.
[24] D. Tamura, K. Aoi, and K. Tsuchiya, *Contribution of phase resetting to adaptive rhythm control in human walking based on the phase response curves of a neuromusculoskeletal model*, Front. Neurosci., *14* (2020), 17.
[25] Q. Yang, F. Liu, and I. Turner, *Numerical methods for fractional partial differential equations with Riesz space fractional derivatives*, Appl. Math. Model., *34*(1) (2010), 200–218.
[26] M. Yavuz, A. Ozdemir, and H. Koca, *A new modeling of fractional-order and sensitivity analysis for hepatitis-B disease with real data*, Fract. Fract., *7*(3) (2023), 165.
[27] T. T. Yusuf and F. Benyah, *Optimal control of vaccination and treatment for an SIR epidemiological model*, World J. Model. Simul., *8*(3) (2012), 194–204.